Interannual variation, decadal trend, and future change in ozone outflow from East Asia

Jia Zhu[1,2] , Hong Liao[3,4] , Yuhao Mao[3], Yang Yang[5], and Hui Jiang[6]

[1]State Key Laboratory of Atmospheric Boundary Layer Physics and Atmospheric Chemistry (LAPC), Institute of Atmospheric Physics, Chinese Academy of Sciences, Beijing, China
[2]University of Chinese Academy of Sciences, Beijing, China
[3]School of Environmental Science and Engineering, Nanjing University of Information Science & Technology, Nanjing, China
[4]Joint International Research Laboratory of Climate and Environment Change, Nanjing University of Information Science & Technology, Nanjing, China
[5]Atmospheric Science and Global Change Division, Pacific Northwest National Laboratory, Richland, Washington, USA
[6]National Meteorological Information Center, China Meteorological Administration, Beijing, China

Correspondence to: Hong Liao (hongliao@nuist.edu.cn)

Abstract. We examine the past and future changes in O_3 outflow from East Asia using a global three-dimensional chemical transport model GEOS-Chem. The simulations of Asian O_3 outflow for 1986–2006 are driven by the assimilated GEOS-4 meteorological fields, and those for 2000–2050 are driven by the meteorological fields archived from the Goddard Institute for Space Studies (GISS) General Circulation Model (GCM) 3 under the IPCC SRES A1B scenario. Sensitivity studies are conducted to examine the respective impacts of meteorological parameters and emissions on the variations in the outflow flux of O_3. Evaluation of the model results against measurements shows that the GEOS-Chem model captures fairly well the seasonal cycles and interannual variations of tropospheric O_3 concentrations, with high correlation coefficients of 0.82–0.93 at four ground-based sites and of 0.55–0.88 at two ozonesonde sites where observations are available. The increasing trends in surface-layer O_3 concentrations in East Asia over the past two decades are captured by the model, although the modeled O_3 trends have low biases. When both meteorological parameters and anthropogenic emissions varied during 1986–2006, the simulated Asian O_3 outflow fluxes exhibited a statistically insignificant decadal trend, but large interannual variations (IAVs) with seasonal absolute percent departure from the mean (APDM) values of 4–9 % and annual APDM value of 3.3 %. Sensitivity simulations indicated that the large IAVs of O_3 outflow fluxes were mainly caused by the variations in meteorological conditions. Variations in meteorological parameters drove the IAVs in O_3 outflow fluxes by altering O_3 concentrations over East Asia and by altering zonal winds, and the latter was identified to be the key factor since the O_3 outflow was highly correlated with zonal winds during 1986–2006. The simulations of the 2000–2050 changes show that the annual

outflow flux of O_3 will increase by 2.0 %, 7.9 %, and 12.2 %, respectively, owing to climate change alone, emissions change alone, and changes in both climate and emissions. Therefore, climate change will aggravate the effects of the increases in anthropogenic emissions on future changes in the Asian O_3 outflow. Future climate change is predicted to greatly increase Asian O_3 outflow in the spring and summer seasons as a result of the projected increases in zonal winds. Findings from the present study help to understand the variations in tropospheric O_3 in the downwind regions of East Asia on different timescales, and have important implications for long-term air quality planning for the downwind regions of China, such as Japan and US.

1 Introduction

Tropospheric ozone (O_3) is an important air pollutant, which has a detrimental effect on human health (Fann et al., 2012; Jhun et al., 2014), crops (Wilkinson et al., 2011; Tai et al., 2014), and ecosystems (Fuentes et al., 2013; Yue and Unger, 2014). It is also an important greenhouse gas that directly contributes to global warming (IPCC, 2013). O_3 has a relatively long lifetime of weeks in the free troposphere (Young et al., 2013; Monks et al., 2015), which makes intercontinental transport of O_3 an important issue for understanding O_3 concentrations and planning emission control measures.

A number of previous studies have shown that Asian continental outflow impacts the global O_3 budget (Liu et al., 2002), and influences O_3 air quality in the downwind regions, such as the western North Pacific through the western North America (Jacob et al., 1999; Tanimoto et al., 2005; Kim et al., 2006; Li et al., 2008; Zhang et al., 2008; Chiang et al., 2009; Kurokawa et al., 2009; Huang et al., 2010; Nagashima et al., 2010; Walker et al., 2010; Ambrose et al., 2011; Lin et al., 2012; Ou-Yang et al., 2013; Han et al., 2015; Pochanart et al., 2015). Liu et al. (2002) reported that boundary-layer O_3 pollution was lifted into the upper troposphere by deep convection over the Asian maritime continent, from where it was transported northward along the upper branch of the local Hadley circulation and into the mid-latitude westerlies, influencing the global O_3 budget. Using a global 3-D chemical transport model GEOS-Chem, Zhang et al. (2008) estimated that Asian pollution enhanced surface-layer O_3 concentrations by 5–7 ppbv over western North America in spring 2006. Walker et al. (2010) used the same model (GEOS-Chem) to evaluate sensitivities of tropospheric O_3 over Canada to Asian anthropogenic emissions, and reported that the contribution from Asian emissions to O_3 profiles above Whistler, Canada, was 6–8 ppbv in spring 2006. Through an integrated analysis of in situ and satellite measurements in May–June 2010 with a global chemistry-climate model GFDL AM3, Lin et al. (2012) reported that Asian emissions could contribute 8–15 ppbv O_3 over the western United States on days when the observed daily maximum 8-h average O_3 (MDA8 O_3) exceeded 60 ppbv, and that 20 % of MDA8 O_3 exceedances of 60 ppbv would not have occurred in the southwestern United States in the absence of Asian anthropogenic emissions.

Asian O_3 outflow exhibits seasonal variations (Liu et al., 2002; Han et al., 2015). Using a global 3-D chemical transport model GEOS-Chem, Liu et al. (2002) simulated the seasonal variations of the Asian outflow flux of O_3 over the Pacific, which was defined as the eastward flux integrated for the tropospheric column through a wall located at 150 °E between 10 °N and 60 °N. They found that the Asian O_3 outflow flux reached the maximum in early spring (March) and the minimum in summer (July). Han et al. (2015) examined O_3 measurements at Ieodo Ocean Research Station, which was located in the East China Sea and regarded as an ideal place to observe Asian outflow without local effects. They reported that the seasonal variation of O_3 was distinct, with a minimum in August and two peaks in April and October, and was greatly affected by the seasonal wind pattern over East Asia.

Continental outflow of O_3 is expected to vary on interannual to decadal timescales, because tropospheric O_3 concentrations and meteorological parameters have variations on these timescales. Large interannual variations (IAVs) of tropospheric O_3 concentrations have been reported in previous observational studies (Kurokawa et al. 2009; Zhou et al., 2013). Analyzing 11 years of ozonesonde data over Hong Kong, Zhou et al. (2013) reported that observed tropospheric O_3 levels during 2000–2010 exhibited high IAV, with an annual averaged amplitude [defined as (maximum + 2nd maximum − minimum − 2nd minimum) × 0.5 / the average during 2000–2010] up to 30 % of the averaged concentrations at 3–8 km altitude. Kurokawa et al. (2009) analyzed observed springtime O_3 over Japan during 1985–2005, and found that the observed O_3 showed greater year-to-year variations than the annual rate of the long-term trend. Decadal trends of tropospheric O_3 concentrations have been reported for different locations on the basis of observations (Ding et al., 2008a; Xu et al., 2008; Tang et al., 2009; Tanimoto, 2009; Wang et al., 2009b; Cooper et al., 2010; Wang et al., 2012; Lin et al., 2014, 2015; Zhang et al., 2014), such as −0.56 ppbv yr^{-1} over Linan in eastern China (Xu et al., 2008), +0.58 ppbv yr^{-1} over Hong Kong in southern China (Wang et al., 2009b), +1.0 ppbv yr^{-1} at Mt. Happo in Japan (for springtime O_3; Tanimoto, 2009), and +0.35 ppbv yr^{-1} over Hawaii in North Pacific (for autumn O_3; Lin et al., 2014). Asian NO_x emissions almost doubled over the past 20 years (Yang et al., 2015), which contributed to the raised O_3 observed over the downwind regions of Asia (Lin et al., 2016).

Future changes of tropospheric O_3 concentrations have also been predicted by modeling studies (Racherla and Adams, 2006, 2009; Lin et al., 2008; Wu et al., 2008a; Lam et al., 2011; Wild et al., 2012; Gao et al., 2013; Liu et al., 2013; Wang et al., 2013; Lee et al., 2015; Val Martin et al., 2015; Schnell et al., 2016; Zhu and Liao, 2016). Wang et al. (2013), using the NASA GISS GCM/GEOS-Chem model combination, reported that the summer surface-layer O_3 levels averaged over China would increase by 11.9 ppbv due to the combined changes in climate and emissions over 2000–2050 under the SRES A1B scenario.

Meteorological parameters, especially winds that are important for O_3 outflow, also exhibit variations on different time scales (Chang et al., 2000; Ding et al., 2008b; Sun et al., 2009; Zhang and Guo, 2010; Hirahara et al., 2012).

Large IAVs of the East Asian summer monsoon (EASM) have been reported in previous studies (Zhu et al., 2012; Yang et al., 2014). The decadal-scale weakening of the EASM since the 1950s has also been reported by many previous studies, and anomalous northeasterlies during the weak monsoon years were found over the western North Pacific near 40 °N, which did not favor the outflow of pollutants from northern China (Chang et al., 2000; Ding et al., 2008b; Zhu et al., 2012). On the basis of NCEP/NCAR reanalysis data, Sun et al. (2009) showed that the axis location of the East Asia subtropical westerly jet (EASWJ) had displaced southward since the end of the 1970s, intensifying the westerly wind over 25–35 °N and weakening it over 42–50 °N, and therefore influencing the outflow of pollutants. Lin et al. (2014) reported that interannual variability in springtime Asian O_3 transport, as inferred by the East Asian COt (carbon-monoxide-like tracer), was strongly influenced by ENSO-related shifts in the subtropical jet stream, and that the decrease in ozone-rich Eurasian airflow reaching the eastern North Pacific during spring in the 2000s was attributed to more frequent La Nina events. Most of the Coupled Model Intercomparison Project Phase 3 (CMIP3) models projected that the Asian jet would be intensified on its equatorward side by the end of the 21st century (Zhang and Guo, 2010; Hirahara et al., 2012).

Few previous studies have examined the IAVs, decadal trends, and future changes in O_3 outflow. In this work, we examine the historical (1986–2006) and future (2000–2050) changes of O_3 outflow from East Asia, and systematically quantify the roles of meteorological parameters and/or anthropogenic emissions on the changes. The descriptions of the model, emissions, and numerical simulations are presented in Sect. 2. Section 3 evaluates the model performance for tropospheric O_3. Section 4 discusses the IAVs and decadal trends in the O_3 outflow from East Asia over 1986–2006. Future changes in O_3 outflow from East Asia for 2000–2050 are presented in Sect. 5.

2 Methods

2.1 Model description

We apply the global 3-D chemical transport model GEOS-Chem to simulate O_3 outflow fluxes. The GEOS-Chem model includes a detailed simulation of O_3–NOx–hydrocarbon (~80 species, ~300 chemical reactions) (Bey et al., 2001) and aerosol chemistry. Aerosol species include sulfate (SO_4^{2-}), nitrate (NO_3^-), ammonium (NH_4^+) (Park et al., 2004; Pye et al., 2009), black carbon (BC) and organic carbon (OC) (Park et al., 2003), mineral dust (Fairlie et al., 2007), and sea salt (Alexander et al., 2005). The simulations account for the impacts of aerosols on the distributions and concentrations of O_3 through heterogeneous reactions and changes in photolysis rates (Lou et al., 2014).

To simulate historical changes in the Asian outflow of O_3, the GEOS-Chem model is driven by the assimilated GEOS-4 meteorological fields from the Goddard Earth Observing System (GEOS) of NASA Global Modeling and

Assimilation Office (GMAO). We perform simulations for 1986–2006, which are the years with available GEOS-4 meteorological datasets. The version of the model used here has a horizontal resolution of 2 ° (latitude) × 2.5 ° (longitude), with 30 vertical layers.

To simulate future changes of O_3 outflow fluxes during 2000–2050, the GEOS-Chem simulation is driven by meteorological data from the National Aeronautics and Space Administration/Goddard Institute for Space Studies (NASA/GISS) general circulation model (GCM) 3 (Rind et al., 2007) for both the present day (1996–2005) and future (2046–2055), following Wu et al. (2008b), Pye et al. (2009), Wang et al. (2013), and Jiang et al. (2013). Both the GISS and GEOS-Chem models used here have a horizontal resolution of 4 °latitude by 5 °longitude, with 23 vertical layers.

2.2 Emissions

For simulations during 1986–2006, the global anthropogenic emissions of reactive nitrogen oxides (NO_x), carbon monoxide (CO), and sulfur dioxide (SO_2) in the model are from the Emission Database for Global Atmospheric Research (EDGAR) inventory (Olivier and Berdowski, 2001). The global emissions of non-methane volatile organic compounds (NMVOCs) are from the Global Emissions Inventory Activity (GEIA) inventory (Piccot et al., 1992). Global emissions of carbonaceous aerosols (BC and OC) follow Bond et al. (2007). Anthropogenic emissions of reactive NO_x, CO, SO_2, NH_3, and NMVOCs over East Asia are overwritten by the emissions inventory of Streets et al. (2003) and Zhang et al. (2009). IAVs of anthropogenic emissions are represented by global-gridded annual scaling factors as described by van Donkelaar et al. (2008) for NO_x, CO, and NMVOCs. Biomass burning emissions are taken from the Global Fire Emissions Database-3 (GFED-3) inventory (van der Werf et al., 2010) for 1997–2006. The biomass burning emissions before 1997 are unavailable because of the lack of datasets.

Figure 1 shows the evolution of anthropogenic and biomass burning emissions of O_3 precursors (NO_x, CO, NMVOCs) summed over the globe and Asia (60–150 ° E, 10 ° S–55 ° N) over 1986–2006. Global anthropogenic emissions of these precursors exhibited no significant trends, while the Asian anthropogenic emissions showed large increases over the past two decades. Relative to year 1986, the Asian anthropogenic emissions of NO_x, CO, and NMVOCs in 2006 increased by 70.0 %, 42.1 %, and 50.9 %, respectively. Compared with anthropogenic emissions, biomass burning emissions had greater IAVs during 1997–2006. Figure 1 also shows the pathway for the global CH_4 abundance used in our simulations of O_3. The CH_4 mixing ratio in 1986 was 1672 ppb, which increased by 6.3 % in 2006. Note that, over 1996–2006 when NO_x emissions and satellite NO_2 columns were simultaneously available, the trend in NO_x emissions over East-Central China (ECC, 110–123 ° E, 30–40 ° N) was +8.2% yr^{-1} on the basis of the emission inventory used in this study, close to the trend of +9.0% yr^{-1} in NO_2 columns averaged over ECC on the basis

of tropospheric NO_2 vertical column density (VCD) data retrieved from GOME (1996–2002) and SCIAMACHY (2003–2006), which are available from www.temis.nl.

For future simulations during 2000–2050, anthropogenic emissions of O_3 precursors, including NO_x, CO, and NMVOCs, are taken from Wu et al. (2008b), and those of NH_3 and SO_2 follow those in Pye et al. (2009). The future anthropogenic emissions of O_3 precursors, aerosol precursors, and aerosols under the SRES A1B scenario are generated by the Integrated Model to Assess the Greenhouse Effect (IMAGE) socioeconomic model using growth factors for different species and countries (Streets et al., 2004). Table 1 shows the present-day (year 2000) and future (year 2050) anthropogenic emissions of O_3 precursors under the SRES A1B scenario. The global emissions of NO_x, CO, and NMVOCs are projected to increase by 78.4 %, 26.4 %, and 89.4 % over 2000–2050; and the Asian emissions are projected to increase by 159.6 %, 23.7 %, and 118.6 %, respectively. Present-day methane mixing ratios are specified as 1750 ppbv on the basis of observations (Wu et al., 2008b). The future methane concentrations are set to 2400 ppbv, following the SRES A1B scenario (Pye et al., 2009).

The natural emissions of O_3 precursors, including NO_x from lighting and soil, and NMVOCs from vegetation, are calculated on the basis of the assimilated GEOS-4 meteorological fields and GISS Model 3 meteorological parameters. The lightning NO_x emissions follow Price and Rind (1992), with the NO_x vertical profile proposed by Pickering et al. (1998). The soil NO_x emissions scheme in the GEOS-Chem model is based on the work of Yienger and Levy (1995) and Wang et al. (1998). Biogenic emissions of NMVOCs are calculated according to the Model of Emissions of Gases and Aerosols from Nature (MEGAN) (Guenther et al., 2006). Figure 2 shows the evolution of natural emissions summed over the globe and Asia over 1986–2006. Both global and Asian NO_x emissions from lightning exhibited large IAVs and significant increasing trends. It has been shown that warming climate leads to increased lightning NO_x (IPCC, 2013). Compared with lightning NO_x emissions, NO_x emissions from soil showed smaller IAVs and no significant decadal trend. Both global and Asian biogenic emissions of NMVOCs have been shown to have large IAVs, as a result of the changes in both vegetation and meteorological parameters (Fu and Liao, 2012). For future simulations during 2000–2050, the natural emissions of O_3 precursors are listed in Table 2. The simulated emissions of lightning NO_x, soil NO_x, and biogenic VOCs are projected to increase by 18.8 %, 14.9 %, and 22.1 % for the globe, and by 16.7 %, 21.4 %, and 18.9 % for Asia, respectively.

The effects of changes in stratosphere–troposphere exchange (STE) of O_3 are not included in this study for both past and future simulations. The cross-tropopause O_3 flux is represented by the synthetic O_3 (Synoz) method (McLinden et al., 2000), which imposes a global annual mean cross-tropopause O_3 flux of 500 Tg yr^{-1}.

2.3 Numerical experiments

To examine the respective and combined impacts of meteorological parameters, anthropogenic emissions, and biomass burning emissions on the IAVs and decadal trends of O_3 outflow from East Asia during 1986–2006, we perform simulations for four cases (Table 3):

(a) Met: The simulation of O_3 outflow for 1986–2006, to examine the effect of variations in meteorological parameters alone. The meteorological parameters vary from 1986 to 2006, and the anthropogenic emissions are fixed at year 2006 levels. Biomass burning emissions are turned off.

(b) Emis: The simulation of O_3 outflow for 1986–2006, to examine the effect of variations in anthropogenic emissions alone. The anthropogenic emissions vary from 1986 to 2006, and the meteorological parameters are fixed at year 2006 levels. Biomass burning emissions are turned off.

(c) MetEmis: The simulation of O_3 outflow for 1986–2006, with variations in both meteorological parameters and anthropogenic emissions during 1986–2006. Biomass burning emissions are turned off.

(d) MetEmisB: The simulation of O_3 outflow for 1997–2006, with variations in meteorological parameters, anthropogenic emissions, and biomass burning emissions during 1997–2006. Note that biomass burning emissions in the model are not available before 1997.

To identify the relative roles of future changes in meteorological parameters and emissions in 2000–2050 changes in Asian O_3 outflow flux, another four simulations are carried out: (a) Met2000Emis2000: present-day climate and emissions; (b) Met2050Emis2000: future climate and present-day anthropogenic emissions; (c) Met2000Emis2050: present-day climate and future anthropogenic emissions; and (d) Met2050Emis2050: future climate and emissions. Both the future climate and anthropogenic emissions follow the IPCC SRES A1B scenario.

The mass flux of O_3 through the vertical plane along 135 °E from 20 °N to 55 °N from the surface to 100 hPa is used to quantify Asian O_3 outflow. The metric of mass flux through a vertical plane was also used by Liu et al. (2002) to represent Asian O_3 outflow, and by Jiang et al. (2013) and Yang et al. (2015) to represent Asian aerosol outflow. It should be noted that the O_3 outflow flux from East Asia includes the effects of emissions in different regions of the world owing to the relatively long lifetime (~3 weeks) of O_3 (Fiore et al., 2002; Liao et al., 2006). However, Liu et al. (2002) found that anthropogenic sources in Asia made the largest contribution to the Asian outflow flux of O_3.

3 Model evaluation

The GEOS-Chem simulations of O_3 have been evaluated extensively for the U.S. (Liu et al., 2006; Wu et al., 2008b; Zhang et al., 2008), Europe (Auvray and Bey, 2005; Liu et al., 2006; Kim et al., 2015), and China (Wang et al., 2013; Lou et al., 2014; Yang et al., 2014; Zhu and Liao, 2016). These studies showed that the GEOS-Chem model captured

the magnitude and distribution of the surface-layer concentration and column burden of tropospheric O_3 fairly well. The vertical distributions of O_3 have also been evaluated by aircraft campaigns and ozonesonde measurements (Zhang et al., 2008; Walker et al., 2010; Wang et al., 2011), showing that the GEOS-Chem model closely reproduced the observed O_3 profiles.

Here, we conduct comparisons with measurements to evaluate whether the version of the GEOS-Chem model used in this study can capture the temporal variations of tropospheric O_3. We use observations of tropospheric O_3 available in East Asia as summarized in Table 4. Observations at two sites (Minamitorishima and Yonagunijima) are from the World Data Centre for Greenhouse Gases (WDCGG, www.ds.data.jma.go.jp/gmd/wdcgg/), and those at another two sites (Rishiri and Ogasawara) are from the Acid Deposition Monitoring Network in East Asia (EANET, www.eanet.asia/product/index.html), which are used to evaluate the simulated surface-layer O_3 concentrations. The four Japanese sites are "remote" sites in the downwind regions of China. Figure 3 compares the time series of monthly surface-layer O_3 mixing ratios simulated by MetEmisB with those measured by WDCGG and EANET. Simulated surface-layer O_3 levels agree well with observations at all the four stations. The model captures fairly well the seasonal cycles and interannual variations of surface O_3, with high correlation coefficients of 0.82–0.93 (Table 4). Generally, the GEOS-Chem model can capture the high values during early spring or winter when Asian O_3 outflow flux is the highest, but overestimates the low values during summer when Asian O_3 outflow is the minimum.

To evaluate the simulated O_3 concentrations for the boundary layer, middle and upper troposphere, we use the ozonesonde data at two Japanese sites from World Ozone and Ultraviolet Radiation Data Centre (WOUDC, www.woudc.org). The information for the two sites (Naha and Tsukuba) is listed in Table 4. Figure 4 compares the time series of monthly O_3 mixing ratios simulated by MetEmisB with those measured by ozonesonde. Comparisons are shown for four altitudes in the troposphere. The GEOS-Chem model captures the seasonal cycles and interannual variations of tropospheric O_3 at all altitudes, with correlation coefficients ranging from 0.68 to 0.88 for Naha site, and from 0.55 to 0.76 for Tsukuba site. However, the agreement with ozonesonde in the lowermost layer (1000–850 hPa) seems to be poorer than that with WDCGG or EANET. It is noted that, the ground-based measurements (WDCGG or EANET) and simulation results are calculated from continuous data, while the ozonesondes are regularly launched at a fixed local time with a typical frequency of 1–2 weeks (Tanimoto et al., 2015). The inconsistency in sampling time may be responsible for the poorer agreement with ozonesonde.

The increasing trend in surface-layer O_3 in East Asia over the past two decades was reported by previous studies (Ding et al., 2008a; Wang et al., 2009b; Xu et al., 2016). Figure 5 compares the simulated trends in seasonal or annual mean surface-layer O_3 concentrations from the MetEmis experiment with the observed trends collected from previous studies. Simulated O_3 concentrations exhibit statistically significant increasing trends at all sites except for Waliguan in

winter, although the model underestimates the trends for some stations and seasons. The modeled O_3 trends were also reported to have low biases in previous studies (Tanimoto et al., 2009; Parrish et al., 2014; Strode et al., 2015). Parrish et al. (2014) compared O_3 trends simulated by three chemistry-climate models with observations at Asian sites, and reported that one model captured less than one third of the observed increasing trend whereas the other two models suggested no significant increasing trends.

In general, the GEOS-Chem model can capture fairly well the seasonal cycles and interannual variations of tropospheric O_3, although the model overestimates the low values during summer indicating an overestimation of Asian O_3 outflow in summer. The increasing trends in surface-layer O_3 in China over the past two decades can also be captured by GEOS-Chem model, although the modeled O_3 trends have low biases.

4 Simulated Asian O_3 outflow during 1986–2006

4.1 Seasonal patterns of Asian O_3 outflow

Figure 6 shows the pressure–latitude cross-sections along 135 °E of the seasonal O_3 outflow fluxes averaged over 1997–2006 in the MetEmisB simulation. The maximum O_3 fluxes were found in the middle-upper troposphere, in consistent with Liu et al. (2002) and Wang et al. (2009a), and it could be attributed to the vertical distributions of both zonal winds and O_3 concentrations. The westerlies strengthen with altitudes with the strongest winds occurring around 200 hPa (known as the East Asia subtropical westerly jet) (Ren et al., 2011). Concentrations of O_3 are high in the upper troposphere over the mid-latitudes (Wang, 1999).

The seasonal mass fluxes through the meridional plane (along 135 °E from 20 °N to 55 °N, and from the surface to 100 hPa) were calculated to be 509.6, 437.6, 126.6, and 268.7 Tg season^{-1} for December–January–February (DJF), March–April–May (MAM), June–July–August (JJA), and September–October–November (SON), respectively. Although the seasonal flux was highest in DJF, the monthly O_3 flux through the panel peaked in March and reached the nadir in July (not shown in Fig. 6). Such monthly variations of the Asian O_3 outflow flux agreed with those in Liu et al. (2002). The maximum O_3 outflow in March was caused by the combined effects of meteorological conditions, biomass burning emissions, and stratospheric O_3 intrusion. The "warm conveyor belt" (WCB) airstreams that export pollution from the Asian boundary layer to the free troposphere, and the mid-latitude prevailing westerly winds in the free troposphere that transport pollution from Asia to the Northwest Pacific, were strongest during the early spring period (Eckhardt et al., 2004; Pochanart et al., 2004). The contribution from Asian biomass burning emissions on O_3 outflow was maximum in the spring and insignificant during other seasons (Liu et al., 2002). The stratospheric O_3 intrusion was also found to be most effective in late winter and early spring (Danielsen and Mohnen, 1977; Mahlman and

Moxim, 1978).

4.2 IAVs and decadal trends of Asian O_3 outflow

Figure 7a shows the simulated annual O_3 outflow fluxes through the meridional plane along 135 °E from 20 °N to 55 °N, from the surface to 100 hPa, during 1986–2006 in the Met, Emis, and MetEmis simulations, and Fig. 7b shows the associated deviations from the mean (DEV). The simulations of the O_3 outflow in Met, Emis, and MetEmis examined, respectively, the effects of variations in meteorological parameters alone, anthropogenic emissions alone, and both meteorological parameters and anthropogenic emissions. The outflow fluxes of O_3 with changes in anthropogenic emissions alone (the Emis simulation) exhibited a statistically significant ($P < 0.001$) increasing trend. However, the magnitude of the increasing trend was very small; the decadal trend of the Asian O_3 outflow flux in the Emis simulation was calculated to be +16.7 Tg decade^{-1} (i.e., +1.2 % decade^{-1}) using the linear fit with least-squares method. The DEV, defined as

$$\mathrm{DEV} = 100\% \times \left(C_i - \frac{1}{n}\sum_{i=1}^{n} C_i\right) / \left(\frac{1}{n}\sum_{i=1}^{n} C_i\right),$$

where n is the number of years examined (n = 21 for 1986–2006) and C_i is the simulated O_3 outflow flux in year i, changed from −1.3 % (in 1986) to +1.4 % (in 2006), also indicating a small increasing trend in the O_3 outflow flux. With variations in meteorological parameters alone (the Met simulation), simulated O_3 outflow fluxes exhibited large IAVs, but a statistically insignificant ($P > 0.05$) decadal trend of −3.4 % decade^{-1}. The DEV values in the Met simulation ranged from −8 % to +16.5 %. With variations in both anthropogenic emissions and meteorological parameters (the MetEmis simulation), the simulated O_3 outflow showed large IAVs, but a statistically insignificant ($P >$ 0.05) decadal trend of −2.2 % decade^{-1}.

To analyze the IAVs of O_3 outflow fluxes, the decadal trend obtained from the linear fit was removed from the time series of simulated O_3 outflow fluxes, following the approach used in previous studies that examined IAVs of aerosol outflow fluxes (Yang et al., 2015) and O_3 concentrations (Camp et al., 2003). The deviations from the mean of the detrended O_3 outflow fluxes from the Met, Emis, and MetEmis simulations over 1986–2006 are shown in Fig. 7c. While the detrended outflow fluxes of O_3 in Met and MetEmis simulations showed large IAVs with DEV values in the range of −7.5 % to +13.5 %, the DEV values in the Emis simulation were very small (in the range of ±0.3 %). The two deviation curves from the Met and MetEmis simulations almost coincided with each other, indicating the dominant role of variations in meteorological parameters in the IAVs of the Asian O_3 outflow flux.

The IAVs in the O_3 outflow fluxes were further quantified with statistical variables of mean absolute deviation (MAD) and absolute percent departure from the mean (APDM), which have been used in previous IAV studies, such

as Mu and Liao (2014), Lou et al. (2015), and Yang et al. (2015). The absolute IAVs of the O_3 outflow fluxes can be quantified by MAD, defined as

$$\mathrm{MAD} = \frac{1}{n}\sum_{i=1}^{n} |C_i - \frac{1}{n}\sum_{i=1}^{n} C_i\,|,$$

while the IAVs relative to the multi-year average outflow flux can be quantified by APDM, defined as

$$\mathrm{APDM} = 100\% \times \mathrm{MAD} / \left(\frac{1}{n}\sum_{i=1}^{n} C_i\right),$$

where n is the number of years examined (n = 21 for years 1986–2006) and C_i is the detrended O_3 outflow flux in year i. The MAD and APDM values of the detrended seasonal and annual O_3 outflow fluxes across the meridional plane along 135 °E from 20 °N to 55 °N, from the surface to 100 hPa, are shown in Fig. 8. The seasonal MAD and APDM values in the Emis simulation were close to zero, while those in the Met and MetEmis simulations were relatively large. The APDM values in the Met and MetEmis simulations were maximum in JJA and minimum in SON. The MAD and APDM values in the Met simulation were almost identical to those in the MetEmis simulation, which indicated again that the IAVs of the O_3 outflow fluxes were mainly dependent on the variations in meteorological conditions, rather than the variations in anthropogenic emissions. With variations in both meteorological parameters and anthropogenic emissions, the seasonal APDM values were in the range of 4–9 % and the annual APDM value was 3.3 %.

Figure 9 shows the pressure–latitude cross-sections of MAD values along 135 °E for detrended annual O_3 outflow fluxes from the Met, Emis, and MetEmis simulations. The O_3 outflow in the Met simulation exhibited large IAVs throughout the whole troposphere, with MAD values greater than 0.2 kg yr^{-1} m^{-2}. The MAD values increased with altitude, which could be attributed to the vertical distributions of the IAVs in westerly winds (see MAD values of winds in Fig. 9a). The variations in anthropogenic emissions led to very small IAVs, with MAD values less than 0.2 kg yr^{-1} m^{-2} (Fig. 9b) throughout the troposphere. With both variations in meteorological parameters and anthropogenic emissions, the MAD values (Fig. 9c) showed almost identical magnitudes and spatial distributions to those in the Met simulation (Fig. 9a), indicating the dominant role of variations in meteorological conditions in the IAVs of the O_3 outflow.

Variations in meteorological conditions can influence the IAVs of the O_3 outflow fluxes by changing O_3 concentrations over East Asia (Yang et al., 2014; Lou et al., 2015), and by altering zonal winds (Kurokawa et al., 2009). The O_3 outflow flux is simulated to correlate positively with zonal wind averaged over 20 °–55 °N along 135 °E, with a high correlation coefficient of +0.71 for annual fluxes and zonal winds. The correlation coefficient between O_3 fluxes and zonal winds is calculated to be +0.96 during summer when the APDM values of O_3 outflow fluxes are maximum. The high correlation coefficients indicate that the variation in zonal winds is the key factor that leads to the large IAVs of O_3 outflow fluxes.

4.3 Effect of variations in biomass burning emissions

The biomass burning emissions of the O_3 precursors exhibited large IAVs during 1997–2006 (Fig. 1). To analyze the impacts of biomass burning emissions on IAVs of O_3 outflow fluxes, we compare the MAD and APDM values of detrended O_3 outflow fluxes during 1997–2006 in the MetEmis and MetEmisB simulations. The MAD (APDM) was calculated to be 31.17 Tg yr^{-1} (2.35 %) in the MetEmis simulation and 31.82 Tg yr^{-1} (2.36 %) in the MetEmisB simulation. The minor influence of biomass burning emissions on the IAVs of the O_3 outflow fluxes from East Asia was also supported by Voulgarakis et al. (2015). Furthermore, Lin et al. (2014) reported that meteorological variability, compared with the variability in biomass burning, was much more important for driving the IAVs in springtime O_3 at the Mauna Loa Observatory, a remote North Pacific site sensitive to Asian pollution outflow.

5 Future changes in Asian O_3 outflow for 2000–2050

In this part of the study, we quantify future decadal changes in Asian O_3 outflow during 2000–2050 under the SRES A1B scenario, and examine the relative impacts of variations in climate and anthropogenic emissions on the changes. We conduct each simulation for 10 years, driven by 1996–2005 meteorology to represent the present-day (year 2000) climate, and by 2046–2055 meteorological fields to represent the future (year 2050) climate, following 1 year of model spin-up. All the results presented below are 10-year averages. Simulated present-day and future changes in seasonal and annual fluxes of O_3 across the vertical plane along 135 °E from 20 °N to 55 °N are summarized in Table 5.

5.1 Present-day O_3 outflow

The pressure–latitude cross-sections along 135 ° E of the simulated present-day (Met2000Emis2000) seasonal O_3 outflow fluxes, driven by the meteorological inputs provided by GISS GCM 3, are shown in Fig. 10a. The magnitudes, spatial distributions, and seasonal variations agree closely with those driven by the assimilated GEOS-4 meteorological fields (Fig. 6). The O_3 outflow flux through the vertical plane is simulated to be 1877.1 Tg yr^{-1} with GISS GCM 3 meteorology, and 1342.5 Tg yr^{-1} with the GEOS-4 assimilated meteorological fields, which indicates the reliability of the simulated present-day O_3 outflow fluxes.

5.2 Effect of future changes in climate alone

Relative to the present-day value, year 2050 annual outflow of O_3 is estimated to increase by 2.0 % (Table 5) as a

result of climate change alone (Met2050Emis2000 minus Met2000Emis2000). The outflow of O_3 shows a slight decrease of 1.8 % in DJF and of 3.8 % in SON, but a large increase of 14.5 % in JJA and of 7.3 % in MAM. The spatial distributions of projected changes in O_3 fluxes are well consistent with those of changes in zonal winds (Fig. 10b). The wind speed of the westerlies in DJF and SON decreases across the troposphere over 30–45 °N, leading to the reductions in the O_3 outflow fluxes. In contrast, the increases in zonal winds in JJA and MAM lead to the increases of O_3 outflow fluxes throughout the troposphere over 30–45 ° N. Our projected future changes in zonal winds are consistent with previous studies. By analyzing 18 CMIP5 models, Huang and Wang (2016) assessed the future changes in atmospheric circulation during spring over East Asia. They found that, although different models projected different changes (even in sign) in zonal winds, the ensemble mean of five better-skill models among the 18 CMIP5 models exhibited overall increases in zonal winds throughout the whole troposphere during spring, which agrees with our simulation. Based on 31 (29)-model ensemble mean results, Jiang and Tian (2013) showed that the westerlies along 135 °E during winter (summer) were projected to weaken (strengthen). Such projected patterns of future changes in westerlies during winter and summer are also captured by our model. Changes in O_3 concentrations also contribute to the changes in O_3 outflow; although the zonal winds are projected to increase north of 40 °N in the upper troposphere during SON, the O_3 outflow fluxes are simulated to decrease because of the significant decreases of O_3 levels north of 40 °N in the upper troposphere (Fig. S1).

5.3 Effect of future changes in anthropogenic emissions alone

The annual outflow of O_3 through the vertical plane is simulated to increase by 7.9 % relative to the present-day value (Table 5) as a result of the changes in anthropogenic emissions alone (Met2000Emis2050 minus Met2000Emis2000). Considering that the O_3 outflow with changes in anthropogenic emissions alone exhibits an increasing trend of 1.2 % decade^{-1} over 1986–2006 (Sect. 4.2), the increasing trend of 1.2 % decade^{-1} (i.e., 6.0 % half-century^{-1}) is close to the value of 7.9 % over the future half-century.

The projected future O_3 fluxes show increases during all seasons, which can be attributed to the increases in O_3 concentrations at all altitudes over Asia and upwind regions (i.e., Europe and Central Asia; Fig. S1) as a result of the increases in anthropogenic emissions of the O_3 precursors (NO_x and NMVOCs) and CH_4 concentrations. NO_x emissions in 2050 are projected to increase by 159.6% over Asia and by 78.4% globally, while NMVOCs emissions are projected to increase by 118.6% over Asia and by 89.4% globally under the SRES A1B scenario (Table 1). The CH_4 mixing ratios are projected to increase by 37.1% relative to the present-day value. The largest increases of O_3 outflow fluxes are located in the middle-upper troposphere (Fig. 10c) owing to the strong westerlies located here. It is

noted that, in spite of the significant increases of emissions, the simulated surface-layer O_3 concentrations show slight decreases over the North China Plain in DJF, which subsequently leads to the small decreases of O_3 outflow fluxes at the surface layer over 30–40 °N. In DJF, biogenic VOC emissions are especially low over the North China Plain, whereas anthropogenic NO_x emissions are fairly high due to the residential heating, leading to a low VOCs/NO_x ratio in this region (Lou et al., 2010; Fu et al., 2012). Therefore, increases in NO_x emissions lead to decreases in surface-layer O_3 concentrations over the North China Plain.

5.4 Effect of future changes in both climate and anthropogenic emissions

The annual outflow of O_3 through the vertical plane is projected to increase by 12.2 % (Table 5) during 2000–2050 as a consequence of future changes in both climate and anthropogenic emissions (Met2050Emis2050 minus Met2000Emis2000). Climate change in DJF and SON slightly offsets the effects of changes in anthropogenic emissions, while climate change in MAM and JJA enhances the effects of variations in anthropogenic emissions. When considering future changes in both emissions and climate, the projected O_3 outflow fluxes show increases throughout almost the entire troposphere along 135 °E during all seasons (Fig. 10d).

6 Uncertainty discussion

There are some uncertainties in our simulations. First, the influence of interannual variation in stratosphere-troposphere exchange on tropospheric O_3 is not considered in this study. Terao et al. (2008) reported that the stratosphere-troposphere exchange had large impacts on the interannual variability of tropospheric O_3 over Canada and Europe but the impact was much smaller over East Asia. The second is the uncertainty associated with the selection of longitudinal transect. We calculate O_3 flux through the vertical plane along 135 °E, because 135 °E is the easternmost boundary of China (i.e., Wusuli River in Northeastern China). We also calculate the O_3 outflow flux along 120 °E, more close to ozone production region in central-eastern China, and find that the variations in O_3 fluxes calculated at 120 °E are similar to those calculated at 135 °E. With variations in both anthropogenic emissions and meteorological parameters (the MetEmis simulation), the simulated O_3 outflow shows large IAVs but a statistically insignificant ($P > 0.05$) trend. The conclusion is consistent with that drawn from the variations in O_3 outflow calculated at 135 °E. Finally, projecting future atmospheric circulation on regional scales has large uncertainty, which is undergoing continuing improvement.

7 Conclusions

We quantify the past and future changes in the O_3 outflow from East Asia using the global 3-D chemical transport model GEOS-Chem. The historical (1986–2006) simulations are driven by the assimilated GEOS-4 meteorological fields, and the future (2000–2050) simulations under the IPCC SRES A1B scenario are driven by the meteorological fields archived from GISS GCM 3. Sensitivity studies are conducted to examine the respective impacts of meteorological parameters and emissions on the variations in the outflow flux.

The measurements from WDCGG and EANET are used to evaluate the simulated surface-layer O_3 concentrations; the ozonesonde data from WOUDC are used to evaluate the simulated O_3 concentrations for the boundary layer, middle and upper troposphere. Generally, the seasonal cycles and interannual variations of tropospheric O_3 concentrations are captured fairly well by the GEOS-Chem model, with high correlation coefficients of 0.82–0.93 at four ground-based sites and 0.55–0.88 at two ozonesonde sites. The increasing trends in surface-layer O_3 concentrations in East Asia over the past two decades can also be captured by the GEOS-Chem model, although the modeled O_3 trends have low biases. Simulated Asian O_3 outflow flux peaks in early spring, and reaches the nadir in summer. The maximum O_3 fluxes are located in the middle-upper troposphere.

The IAVs and decadal trends of Asian O_3 outflow are examined over 1986–2006. Simulated O_3 outflow fluxes showed large IAVs, but an insignificant decadal trend; with variations in both meteorological parameters and anthropogenic emissions, the seasonal APDM values were in the range of 4–9 %. Sensitivity simulations showed that the large IAVs of the O_3 outflow fluxes were mainly caused by the variations in meteorological conditions, rather than the variations in anthropogenic and biomass burning emissions. Although variations in meteorological parameters could influence the IAVs of the O_3 outflow fluxes by changing O_3 concentrations over East Asia and by altering zonal winds, the latter was identified to be the key factor because of the high correlation coefficient of +0.71 between the annual fluxes and zonal winds.

The decadal changes in Asian O_3 outflow are also examined during 2000–2050. The present-day annual O_3 flux through the vertical plane is calculated as 1877.1 Tg, which is projected to change over 2000–2050 by +2.0 %, +7.9 %, and +12.2 %, respectively, due to climate change alone, emissions change alone, and changes in both climate and emissions. During MAM and JJA, climate change plays a larger role in the future changes in O_3 outflow compared with emissions changes, owing to the significant increases in zonal winds during these two seasons. It is noted that climate change will aggravate the impacts of increases in anthropogenic emissions on the O_3 outflow from East Asia over 2000–2050 under the SRES A1B scenario.

These findings are helpful for understanding the temporal evolutions of tropospheric O_3 on different timescales in the downwind regions of East Asia. Observed IAVs of tropospheric O_3 on a relatively short timescale can be attributed to variations in meteorological parameters. Furthermore, conclusions from this study will have important implications

for long-term air quality planning for the downwind regions of China, such as Japan and US. Since future climate change will increase O_3 outflow from East Asia, extra efforts are needed to reduce anthropogenic emissions of O_3 precursors to offset the adverse effects caused by climate change.

8 Data availability

GEOS-Chem is an open-access model developed collaboratively at Harvard University and other institutes in North America, Europe, and Asia. The source codes can be downloaded from http://acmg.seas.harvard.edu/geos/. The tropospheric NO_2 vertical column density (VCD) data are retrieved from GOME (1996–2002) and SCIAMACHY (2003–2006), which are available from www.temis.nl. The O_3 measurements at Minamitorishima and Yonagunijima are available from the World Data Centre for Greenhouse Gases (WDCGG, www.ds.data.jma.go.jp/gmd/wdcgg/), and those at Rishiri and Ogasawara are available from the Acid Deposition Monitoring Network in East Asia (EANET, www.eanet.asia/product/index.html). The ozonesonde data at Naha and Tsukuba are available from the World Ozone and Ultraviolet Radiation Data Centre (WOUDC, www.woudc.org). All data presented in this study are available upon request from the corresponding author.

Author contributions. H. Liao and J. Zhu conceived the study and designed the experiments. J. Zhu performed the simulations, carried out the data analysis, and prepared the manuscript. Y. Mao provided useful comments on the paper. Y. Yang and H. Jiang helped with performing the experiments.

Competing interests. The authors declare that they have no conflicts of interest.

Acknowledgements. This work was supported by the National Basic Research Program of China (973 program, Grant No. 2014CB441202) and the National Natural Science Foundation of China under grants 91544219 and 41475137. We acknowledge the free use of GOME and SCIAMACHY tropospheric NO_2 vertical column density (VCD) data available from www.temis.nl. The following data centers are also acknowledged: the World Data Centre for Greenhouse Gases (WDCGG, www.ds.data.jma.go.jp/gmd/wdcgg/) operated by Japan Meteorological Agency (JMA) in cooperation with World Meteorological Organization (WMO); the World Ozone and Ultraviolet Radiation Data Centre (WOUDC, www.woudc.org) operated by Environment Canada for the Global Atmosphere Watch (GAW) program of WMO. The Rishiri and Ogasawara sites are operated by Ministry of the Environment of Japan as part of the Acid Deposition Monitoring Network in East Asia (EANET, www.eanet.asia/product/index.html) program. We are also very grateful to the reviewers for their helpful comments and thoughtful suggestions.

References

Alexander, B., Park, R. J., Jacob, D. J., Li, Q. B., Yantosca, R. M., Savarino, J., Lee, C. C. W., and Thiemens, M. H.: Sulfate formation in sea-salt aerosols: constraints from oxygen isotopes, J. Geophys. Res., 110(D10), D10307, doi:10.1029/2004JD005659, 2005.

Ambrose, J. L., Reidmiller, D. R., and Jaffe, D. A.: Causes of high O_3 in the lower free troposphere over the Pacific Northwest as observed at the Mt. Bachelor Observatory, Atmos. Environ., 45(30), 5302–5315, doi:10.1016/j.atmosenv.2011.06.056, 2011.

Auvray, M., and Bey, I.: Long-range transport to Europe: Seasonal variations and implications for the European ozone budget, J. Geophys. Res., 110, D11303, doi:10.1029/2004JD005503, 2005.

Bey, I., Jacob, D. J., Yantosca, R. M., Logan, J. A., Field, B., Fiore, A. M., Li, Q., Liu, H., Mickley, L. J., and Schultz, M.: Global modeling of tropospheric chemistry with assimilated meteorology: model description and evaluation, J. Geophys. Res., 106(D19), 23073–23095, doi:10.1029/2001JD000807, 2001.

Bond, T. C., Bhardwaj, E., Dong, R., Jogani, R., Jung, S., Roden, C., Streets, D. G., and Trautmann, N. M.: Historical emissions of black and organic carbon aerosol from energy-related combustion, 1850–2000, Global Biogeochem. Cy., 21, GB2018, doi: 10.1029/2006GB002840, 2007.

Camp, C. D., Roulston, M. S., and Yung, Y. L.: Temporal and spatial patterns of the interannual variability of total ozone in the tropics, J. Geophys. Res., 108(D20), 4643, doi:10.1029/2001JD001504, 2003.

Chang, C. P., Zhang, Y., and Li, T.: Interannual and interdecadal variations of the East Asian summer monsoon and tropical Pacific SSTs. Part I: Roles of the subtropical ridge, J. Clim., 13(24), 4310–4325, doi:10.1175/1520-0442(2000)013<4310:IAIVOT>2.0.CO;2, 2000.

Chiang, C. K., Fan, J. F., Li, J., and Chang, J. S.: Impact of Asian continental outflow on the springtime ozone mixing ratio in northern Taiwan, J. Geophys. Res., 114(D24), D24304, doi: 10.1029/2008JD011322, 2009.

Cooper, O. R., Parrish, D. D., Stohl, A., Trainer, M., N ́ed ́elec, P., Thouret, V., Cammas, J. P., Oltmans, S. J., Johnson, B. J., Tarasick, D., Leblanc, T., McDermid, I. S., Jaffe, D., Gao, R., Stith, J., Ryerson, T., Aikin, K., Campos, T., Weinheimer, A., and Avery, M. A.: Increasing springtime ozone mixing ratios in the free troposphere over western North America, Nature, 463, 344–348, doi:10.1038/nature08708, 2010.

Danielsen, E. F., and Mohnen, V. A.: Project Dustorm report: Ozone transport, in situ measurements, and meteorological analyses of tropopause folding, J. Geophys. Res., 82(37), 5867–5877, doi:10.1029/JC082i037p05867, 1977.

Ding, A. J., Wang, T., Thouret, V., Cammas, J. P., and N ́ed ́elec, P.: Tropospheric ozone climatology over Beijing: analysis of aircraft data from the MOZAIC program, Atmos. Chem. Phys., 8, 1–13, doi:10.5194/acp-8-1-2008,

2008a.

Ding, Y., Wang, Z., and Sun, Y.: Inter-decadal variation of the summer precipitation in east China and its association with decreasing Asian summer monsoon. Part I: Observed evidences, Int. J. Climatol., 28(9), 1139–1161, doi:10.1002/joc.1615, 2008b.

Eckhardt, S., Stohl, A., Wernli, H., James, P., Forster, C., and Spichtinger, N: A 15-year climatology of warm conveyor belts, J. Climate, 17, 218–237, doi: 10.1175/1520-0442(2004)017<0218:AYCOWC>2.0.CO;2, 2004.

Fairlie, T. D., Jacob, D. J., and Park R. J.: The impact of transpacific transport of mineral dust in the United States, Atmos. Environ., 41, 1251–1266, doi:10.1016/j.atmosenv.2006.09.048, 2007.

Fann, N., Lamson, A. D., Anenberg, S. C., Wesson, K., Risley, D., and Hubbell, B. J.: Estimating the national public health burden associated with exposure to ambient $PM_{2.5}$ and ozone, Risk Anal., 32, 81–95, doi:10.1111/j.1539-6924.2011.01630.x, 2012.

Fiore, A. M., Jacob, D. J., Bey, I., Yantosca, R. M., Field, B. D., Fusco, A. C., and Wilkinson, J. G.: Background ozone over the United States in summer: Origin, trend, and contribution to pollution episodes, J. Geophys. Res., 107, D15, doi:10.1029/2001JD000982, 2002.

Fu, J. S., Dong, X., Gao, Y., Wong, D. C., and Lam, Y. F.: Sensitivity and linearity analysis of ozone in East Asia: the effects of domestic emission and intercontinental transport, J. Air. Waste. Manag. Assoc., 62(9), 1102–1114, doi: 10.1080/10962247.2012.699014, 2012.

Fu, Y., and Liao, H.: Simulation of the interannual variations of biogenic emissions of volatile organic compounds in China: impacts on tropospheric ozone and secondary organic aerosol, Atmos. Environ., 59, 170–185, doi:10.1016/j.atmosenv.2012.05.053, 2012.

Fuentes, J. D., Tai, H. R., and Zenker, J.: Ozone impedes the ability of a herbivore to find its host, Environ. Res. Lett., 8, 014048, doi:10.1088/1748-9326/8/1/014048, 2013.

Gao, Y., Fu, J. S., Drake, J. B., Lamarque, J.-F., and Liu, Y.: The impact of emission and climate change on ozone in the United States under representative concentration pathways (RCPs), Atmos. Chem. Phys., 13, 9607–9621, doi:10.5194/acp-13-9607-2013, 2013.

Guenther, A., Karl, T., Harley, P., Wiedinmyer, C., Palmer, P. I., and Geron, C.: Estimates of global terrestrial isoprene emissions using MEGAN (Model of Emissions of Gases and Aerosols from Nature), Atmos. Chem. Phys., 6, 3181–3210, doi:10.5194/acp-6-3181-2006, 2006.

Han, J., Shin, B., Lee, M., Hwang, G., Kim, J., Shim, J., Lee, G., and Shim, C.: Variations of surface ozone at Ieodo Ocean Research Station in the East China Sea and the influence of Asian outflows, Atmos. Chem. Phys., 15, 12611–12621, doi:10.5194/acp-15-12611-2015, 2015.

Hirahara, S., Ohno, H., Oikawa, Y., and Maeda, S.: Strengthening of the southern side of the jet stream and delayed withdrawal of Baiu season in future climate, Journal of the Meteorological Society of Japan, 90(5), 663–671, doi: 10.2151/jmsj.2012 ~~-~~506, 2012.

Huang, M., Carmichael, G. R., Adhikary, B., Spak, S. N., Kulkarni, S., Cheng, Y. F., Wei, C., Tang, Y., Parrish, D. D., Oltmans, S. J., D'Allura, A., Kaduwela, A., Cai, C., Weinheimer, A. J., Wong, M., Pierce, R. B., Al-Saadi, J. A., Streets, D. G., and Zhang, Q.: Impacts of transported background ozone on California air quality during the ARCTAS-CARB period–a multi-scale modeling study, Atmos. Chem. Phys., 10, 6947–6968, doi:10.5194/acp-10-6947-2010, 2010.

Huang, W. R., and Wang, S. Y. S.: Future changes in propagating and non-propagating diurnal rainfall over East Asia, Clim. Dyn., 1–15, doi: 10.1007/s00382-016-3348-4, 2016.

IPCC: Climate Change 2013: The Physical Science Basis. Contribution of Working Group I to the Fifth Assessment Report of the Intergovernmental Panel on Climate Change, edited by: Stocker, T. F., Qin, D., Plattner, G. K., Tignor, M., Allen, S. K., Boschung, J., Nauels, A., Xia, Y., Bex, V., and Midgley, P.M., Cambridge Univ. Press, Cambridge, UK and New York, 1–1535, 2013.

Jacob, D. J., Logan, J. A., and Murti, P. P.: Effect of rising Asian emissions on surface ozone in the United States, Geophys. Res. Lett., 26, 2175–2178, doi: 10.1029/1999GL900450, 1999.

Jhun, I., Fann, N., Zanobetti, A., and Hubbell, B.: Effect modification of ozone-related mortality risks by temperature in 97 US cities, Environ. Int., 73, 128–134, doi:10.1016/j.envint.2014.07.009, 2014.

Jiang D. B., and Tian, Z. P.: East Asian monsoon change for the 21st century: Results of CMIP3 and CMIP5 models, Chinese Sci. Bull., 58, 1427–1435, doi:10.1007/s11434-012-5533-0, 2013.

Jiang, H., Liao, H., Pye, H. O. T., Wu, S., Mickley, L. J., Seinfeld, J. H., and Zhang, X. Y.: Projected effect of 2000–2050 changes in climate and emissions on aerosol levels in China and associated transboundary transport, Atmos. Chem. Phys., 13, 7937–7960, doi:10.5194/acp-13-7937-2013, 2013.

Kim, J. H., Lee, H. J., and Lee, S. H.: The characteristics of tropospheric ozone seasonality observed from ozone soundings at Pohang, Korea, Environ. Monit. Assess., 118, 1–12, doi:10.1007/s10661-006-0772-7, 2006.

Kim, M. J., Park, R. J., Ho, C. H., Woo, J. H., Choi, K. C., Song, C. K., and Lee, J. B.: Future ozone and oxidants change under the RCP scenarios. Atmos. Environ., 101, 103–115, doi:10.1016/j.atmosenv.2014.11.016, 2015.

Kurokawa, J., Ohara, T., Uno, I., Hayasaki, M., and Tanimoto, H.: Influence of meteorological variability on interannual variations of springtime boundary layer ozone over Japan during 1981–2005, Atmos. Chem. Phys., 9, 6287–6304, doi:10.5194/acp-9-6287-2009, 2009.

Lam, Y. F., Fu, J. S., Wu, S., and Mickley, L. J.: Impacts of future climate change and effects of biogenic emissions on

surface ozone and particulate matter concentrations in the United States, Atmos. Chem. Phys., 11, 4789–4806, doi:10.5194/acp-11-4789-2011, 2011.

Lee, J. B., Cha, J. S., Hong, S. C., Choi, J. Y., Myoung, J. S., Park, R. J., Woo, J. H., Ho, C., Han, J. S., and Song, C. K.: Projections of summertime ozone concentration over East Asia under multiple IPCC SRES emission scenarios, Atmos. Environ., 106, 335–346, doi:10.1016/j.atmosenv.2015.02.019, 2015.

Li, J., Wang, Z., Akimoto, H., Yamaji, K., Takigawa, M., Pochanart, P., Liu, Y., Tanimoto, H., and Kanaya, Y.: Near-ground ozone source attributions and outflow in central eastern China during MTX2006, Atmos. Chem. Phys., 8, 7335–7351, doi:10.5194/acp-8-7335-2008, 2008.

Liao, H., Chen, W. T., and Seinfeld, J. H.: Role of climate change in global predictions of future tropospheric ozone and aerosols, J. Geophys. Res., 111, D12304, doi:10.1029/2005JD006852, 2006.

Lin, J. T., Patten, K. O., Hayhoe, K., Liang, X. Z., and Wuebbles, D. J.: Effects of future climate and biogenic emissions changes on surface ozone over the United States and China, J. Appl. Meteorol. Climatol., 47, 1888–1909, doi: 10.1175/2007JAMC1681.1, 2008.

Lin, M., Fiore, A. M., Horowitz, L. W., Cooper, O. R., Naik, V., Holloway, J., Johnson, B. J., Middlebrook, A. M., Oltmans, S. J., Pollack, I. B., Ryerson, T. B., Warner, J. X., Wiedeninmyer, C., Wilson, J., and Wyman, B.: Transport of Asian ozone pollution into surface air over the western United States in spring, J. Geophys. Res., 117, D00V07, doi:10.1029/2011JD016961, 2012.

Lin, M., Horowitz, L. W., Cooper, O. R., Tarasick, D., Conley, S., Iraci, L. T., Johnson, B., Leblanc, T., Petropavlovskikh, I., and Yates, E. L.: Revisiting the evidence of increasing springtime ozone mixing ratios in the free troposphere over western North America, Geophys. Res. Lett., 42, 8719–8728, doi:10.1002/2015GL065311, 2015.

Lin, M., Horowitz, L. W., Oltmans, S. J., Fiore, A. M., and Fan, S.: Tropospheric ozone trends at Mauna Loa Observatory tied to decadal climate variability, Nat. Geosci., 7, 136–143, doi:10.1038/ngeo2066, 2014.

Lin, M., Horowitz, L. W., Payton, R., Fiore, A. M., and Tonnesen, G.: US surface ozone trends and extremes from 1980–2014: Quantifying the roles of rising Asian emissions, domestic controls, wildfires, and climate, Atmos. Chem. Phys. Discuss., doi:10.5194/acp-2016-1093, in review, 2016.

Lin, Y.-K., Lin, T.-H., and Chang, S.-C.: The changes in different ozone metrics and their implications following precursor reductions over northern Taiwan from 1994 to 2007, Environ. Monit. Assess., 169, 143–157, doi: 10.1007/s10661-009-1158-4, 2010.

Liu, H., Jacob, D. J., Chan, L. Y., Oltmans, S. J., Bey, I., Yantosca, R. M., Harris, J. M., Duncan, B. N., and Martin, R. V.: Sources of tropospheric ozone along the Asian Pacific Rim: An analysis of ozonesonde observations, J. Geophys.

Res., 107(D21), 4573, doi:10.1029/2001JD002005, 2002.

Liu, Q., Lam, K. S., Jiang, F., Wang, T. J., Xie, M., Zhuang, B. L., and Jiang, X. Y.: A numerical study of the impact of climate and emission changes on surface ozone over South China in autumn time in 2000–2050, Atmos. Environ., 76, 227–237, doi:10.1016/j.atmosenv.2013.01.030, 2013.

Liu, X., Chance, K., Sioris, C. E., Kurosu, T. P., Spurr, R. J., Martin, R. V., Fu, T. M., Logan, J. A., Jacob, D. J., Palmer, P. I., Newchurch, M. J., Megretskaia, I. A., Chatfield, R. B.: First directly retrieved global distribution of tropospheric column ozone from GOME: Comparison with the GEOS-Chem model. J. Geophys. Res. Atmos., 111, D02308, doi:10.1029/2005JD006564, 2006.

Lou, S., Liao, H., and Zhu, B.: Impacts of aerosols on surface-layer ozone concentrations in China through heterogeneous reactions and changes in photolysis rates, Atmos. Environ., 85, 123–138, doi:10.1016/j.atmosenv.2013.12.004, 2014.

Lou, S., Liao, H., Yang, Y., and Mu, Q.: Simulation of the interannual variations of tropospheric ozone over China: Roles of variations in meteorological parameters and anthropogenic emissions, Atmos. Environ., 122, 839–851, doi:10.1016/j.atmosenv.2015.08.081, 2015.

Lou, S., Zhu, B., and Liao, H.: Impacts of O_3 precursor on surface O_3 concentration over China, Chinese Trans. Atmos. Sci., 33, 451–459, 2010.

Mahlman, S. D., and Moxim, W. J.: Tracer simulation using a global general circulation model: Results from a midlatitude instantaneous source experiment, J. Atmos. Sci., 35(8), 1340–1374, doi: 10.1175/1520-0469(1978)035<1340:TSUAGG>2.0.CO;2, 1978.

McLinden, C. A., Olsen, S. C., Hannegan, B., Wild, O., Prather, M. J., and Sundet, J.: Stratospheric ozone in 3-D models: A simple chemistry and the cross-tropopause flux, J. Geophys. Res., 105, 14653–14665, doi:10.1029/2000JD900124, 2000.

Monks, P. S., Archibald, A. T., Colette, A., Cooper, O., Coyle, M., Derwent, R., Fowler, D., Granier, C., Law, K. S., Mills, G. E., Stevenson, D. S., Tarasova, O., Thouret, V., Von Schneidemesser, E., Sommariva, R., Wild, O., Williams, M. L.: Tropospheric ozone and its precursors from the urban to the global scale from air quality to short-lived climate forcer, Atmos. Chem. Phys., 15, 8889–8973, doi:10.5194/acp-15-8889-2015, 2015.

Mu, Q., and Liao, H.: Simulation of the interannual variations of aerosols in China: role of variations in meteorological parameters, Atmos. Chem. Phys., 14, 9597–9612, doi:10.5194/acp-14-9597-2014, 2014.

Nagashima, T., Ohara, T., Sudo, K., and Akimoto, H.: The relative importance of various source regions on East Asian surface ozone, Atmos. Chem. Phys., 10, 11305–11322, doi:10.5194/acp-10-11305-2010, 2010.

Olivier, J. G. J. and Berdowski, J. J. M.: Global emissions sources and sinks, edited by Berdowski, J., Guicherit, R. and

Heij, B. J., in: “The Climate System”, A. A. Balkema Publishers/Swets & Zeitlinger Publishers, Lisse, The Netherlands, ISBN9058092550, 33–78, 2001.

Ou-Yang, C. F., Hsieh, H. C., Wang, S. H., Lin, N. H., Lee, C. T., Sheu, G. R., and Wang, J. L.: Influence of Asian continental outflow on the regional background ozone level in Northern South China Sea, Atmos. Environ., 78, 144–153, doi:10.1016/j.atmosenv.2012.07.040, 2013.

Park, R. J., Jacob, D. J., Chin, M., and Martin, R. V.: Sources of carbonaceous aerosols over the United States and implications for natural visibility, J. Geophys. Res., 108, 4355, doi:10.1029/2002JD003190, 2003.

Park, R. J., Jacob, D. J., Field, B. D., Yantosca, R. M., and Chin, M.: Natural and transboundary pollution influences on sulfate-nitrate-ammonium aerosols in the United States: implications for policy, J. Geophys. Res., 109, D15204, doi:10.1029/2003JD004473, 2004.

Parrish, D. D., et al.: Long-term changes in lower tropospheric baseline ozone concentrations: Comparing chemistry-climate models and observations at northern midlatitudes, J. Geophys. Res., 119(9), 5719–5736, doi: 10.1002/2013JD021435, 2014.

Piccot, S. D., Watson, J. J., and Jones, J. W.: A global inventory of volatile organic compound emissions from anthropogenic sources, J. Geophys. Res., 97, 9897–9912, doi:10.1029/92JD00682, 1992.

Pickering, K. E., Wang, Y. S., Tao, W. K., Price, C., and Muller, J. F.: Vertical distributions of lightning NO_x for use in regional and global chemical transport models, J. Geophys. Res., 103, 31203–31216, doi:10.1029/98JD02651, 1998.

Pochanart, P., Wang, Z., and Akimoto, H.: Boundary Layer Ozone Transport from Eastern China to Southern Japan: Pollution Episodes Observed during Monsoon Onset in 2004, Asian J. Atmos. Environ., 9, 48–56, doi:10.5572/ajae.2015.9.1.048, 2015.

Pochanart, P., Wild, O., and Akimoto, H.: Air pollution import to and export from East Asia, edited by Stohl, A., Hand Book of Environmental Chemistry, Springer, Berlin and Heidelberg, 99–130, 2004.

Price, C., and Rind, D.: A simple lightning parameterization for calculating global lightning distributions, J. Geophys. Res., 97, 9919–9933, doi:10.1029/92JD00719, 1992.

Pye, H. O. T., Liao, H., Wu, S., Mickley, L. J., Jacob, D. J., Henze, D. K., and Seinfeld, J. H.: Effect of changes in climate and emissions on future sulfate-nitrate-ammonium aerosol levels in the United States, J. Geophys. Res., 114, D01205, doi:10.1029/2008JD010701, 2009.

Racherla, P. N., and Adams P. J.: Sensitivity of global tropospheric ozone and fine particulate matter concentrations to climate change, J. Geophys. Res., 111, D24103, doi:10.1029/2005JD006939, 2006.

Racherla, P. N., and Adams, P. J.: U.S. ozone air quality under changing climate and anthropogenic emissions, Environ. Sci. Technol., 43, 571–577, doi:10.1021/es800854f, 2009.

Ren, X., Yang, X., Zhou, T., and Fan, J.: Diagnostic comparison of wintertime East Asian subtropical jet and polar-front jet: Large-scale characteristics and transient eddy activities, Acta Meteorol. Sin., 25, 21–33, doi:10.1007/s13351-011-0002-2, 2011.

Rind, D., Lerner, J., Jonas, J., and McLinden, C.: Effects of resolution and model physics on tracer transports in the NASA Goddard Institute for Space Studies general circulation models, J. Geophys. Res., 112, D09315, doi:10.1029/2006JD007476, 2007.

Schnell, J. L., Prather, M. J., Josse, B., Naik, V., Horowitz, L. W., Zeng, G., Shindell, D. T., and Faluvegi, G.: Effect of climate change on surface ozone over North America, Europe, and East Asia, Geophys. Res. Lett., 43, 3509–3518, doi:10.1002/2016GL068060, 2016.

Streets, D. G., Bond, T. C., Carmichael, G. R., Fernandes, S. D., Fu, Q., Klimont, Z., Nelson, S. M., Tsai, N. Y., Wang, M. Q., Woo, J-H., and Yarber, K. F.: An inventory of gaseous and primary aerosol emissions in Asia in the year 2000, J. Geophys. Res, 108, D21, doi:10.1029/2002JD003093, 2003.

Streets, D. G., Bond, T. C., Lee, T., and Jang, C.: On the future of carbonaceous aerosol emissions, J. Geophys. Res., 109, D24212, doi:10.1029/2004JD004902, 2004.

Strode, S. A., Rodriguez, J. M., Logan, J. A., Cooper, O. R., Witte, J. C., Lamsal, L. N., Damon, M., Van Aartsen, B., Steenrod, S. D., and Strahan, S. E.: Trends and variability in surface ozone over the United States, J. Geophys. Res.-Atmos., 120, 9020–9042, doi:10.1002/2014JD022784, 2015.

Sun, F. H., Zhang, Y. C., and Guo, L. L.: Relationship between the East Asia subtropical westerly jet anomaly and summer precipitation over eastern China, Plateau Meteorology, 28(6), 1308–1315, 2009.

Tai, A. P. K., Val Martin, M., and Heald, C. L.: Threat to future global food security from climate change and ozone air pollution, Nat. Clim. Change., 4, 817–821, doi:10.1038/nclimate2317, 2014.

Tang, G., Li, X., Wang, Y., Xin, J., and Ren, X.: Surface ozone trend details and interpretations in Beijing, 2001–2006, Atmos. Chem. Phys., 9, 8813–8823, doi:10.5194/acp-9-8813-2009, 2009.

Tanimoto, H.: Increase in springtime tropospheric ozone at a mountainous site in Japan for the period 1998–2006, Atmos. Environ., 43, 1358–1363, doi:10.1016/j.atmosenv.2008.12.006, 2009.

Tanimoto, H., Ohara, T., and Uno, I.: Asian anthropogenic emissions and decadal trends in springtime tropospheric ozone over Japan: 1998–2007, Geophys. Res. Lett., 36, L23802, doi:10.1029/2009GL041382, 2009.

Tanimoto, H., Sawa, Y., Matsueda, H., Uno, I., Ohara, T., Yamaji, K., Kurokawa, J., and Yonemura, S.: Significant latitudinal gradient in the surface ozone spring maximum over East Asia. Geophys. Res. Lett., 32, L21805, doi:10.1029/2005GL023514, 2005.

Tanimoto, H., Zbinden, R. M., Thouret, V., and Nédélec, P.: Consistency of tropospheric ozone observations made by

different platforms and techniques in the global databases, Tellus B, 67, 27073, doi:10.3402/tellusb.v67.27073, 2015.

Terao, Y., Logan, J. A., Douglass, A. R., and Stolarski, R. S.: Contribution of stratospheric ozone to the interannual variability of tropospheric ozone in the northern extratropics, J. Geophys. Res., 113, D18309, doi:10.1029/2008JD009854, 2008.

Val Martin, M., Heald, C. L., Lamarque, J.-F., Tilmes, S., Emmons, L. K., and Schichtel, B. A.: How emissions, climate, and land use change will impact mid-century air quality over the United States: A focus on effects at National Parks, Atmos. Chem. Phys., 15, 2805–2823, doi:10.5194/acp-15-2805-2015, 2015.

van der Werf, G. R., Randerson, J. T., Giglio, L., Collatz, G. J., Mu, M., Kasibhatla, P. S., Morton, D. C., DeFries, R. S., Jin, Y., and van Leeuwen, T. T., Global fire emissions and the contribution of deforestation, savanna, forest, agricultural, and peat fires (1997–2009), Atm. Chem. Phys., 10, 11707–11735, doi:10.5194/acp-10-11707-2010, 2010.

van Donkelaar, A., Martin, R. V., Leaitch, W. R., Macdonald, A. M., Walker, T. W., Streets, D. G., Zhang, Q., Dunlea, E. J., Jimenez, J. L., Dibb, J. E., Huey, L. G., Weber, R., and Andreae, M. O.: Analysis of aircraft and satellite measurements from the Intercontinental Chemical Transport Experiment (INTEX-B) to quantify long-range transport of East Asian sulfur to Canada, Atmos. Chem. Phys., 8, 2999–3014, doi:10.5194/acp-8-2999-2008, 2008.

Voulgarakis, A., Marlier, M. E., Faluvegi, G., Shindell, D. T., Tsigaridis, K., and Mangeon, S.: Interannual variability of tropospheric trace gases and aerosols: The role of biomass burning emissions, J. Geophys. Res., 120, 7157–7173, doi:10.1002/2014JD022926, 2015.

Walker, T. W., Martin, R. V., van Donkelaar, A., Leaitch, W. R., MacDonald, A. M., Anlauf, K. G., Cohen, R. C., Bertram, T. H., Huey, L. G., Avery, M. A., Weinheimer, A. J., Flocke, F. M., Tarasick, D. W., Thompson, A. M., Streets, D. G., and Liu, X.: Trans-Pacific transport of reactive nitrogen and ozone to Canada during spring, Atmos. Chem. Phys., 10, 8353–8372, doi:10.5194/acp-10-8353-2010, 2010.

Wang, K., Zhang, Y., Jang, C., Phillips, S., and Wang, B.: Modeling intercontinental air pollution transport over the trans-Pacific region in 2001 using the Community Multiscale Air Quality modeling system, J. Geophys. Res., 114, D04307, doi:10.1029/2008JD010807, 2009a.

Wang, M.: Atmospheric Chemistry (second edition), Meteorological Press of China, Beijing, China, pp.343, 1999.

Wang, T., Wei, X. L., Ding, A. J., Poon, C. N., Lam, K. S., Li, Y. S., Chan, L. Y., and Anson, M.: Increasing surface ozone concentrations in the background atmosphere of Southern China, 1994–2007, Atmos. Chem. Phys., 9, 6217–6227, doi:10.5194/acp-9-6217-2009, 2009b.

Wang, Y., Jacob, D. J., and Logan, J. A.: Global Simulation of tropospheric O_3-NO_x-hydrocarbon chemistry: 1. Model

formulation, J. Geophys. Res., 103, 10713–10725, doi:10.1029/98JD00158, 1998.

Wang, Y., Konopka, P., Liu, Y., Chen, H., Müller, R., Plöger, F., Riese, M., Cai, Z., and Lü, D.: Tropospheric ozone trend over Beijing from 2002–2010: ozonesonde measurements and modeling analysis, Atmos. Chem. Phys., 12, 8389–8399, doi:10.5194/acp-12-8389-2012, 2012.

Wang, Y., Shen, L., Wu, S., Mickley, L., He, J., and Hao, J.: Sensitivity of surface ozone over China to 2000–2050 global changes of climate and emissions, Atmos. Environ., 75, 374–382, doi:10.1016/j.atmosenv.2013.04.045, 2013.

Wang, Y., Zhang, Y., Hao, J., and Luo, M.: Seasonal and spatial variability of surface ozone over China: contributions from background and domestic pollution, Atmos. Chem. Phys., 11, 3511–3525, doi:10.5194/acp-11-3511-2011, 2011.

Wild, O., Fiore, A. M., Shindell, D. T., Doherty, R. M., Collins, W. J., Dentener, F. J., Schultz, M. G., Gong, S., MacKenzie, I. A., Zeng, G., Hess, P., Duncan, B. N., Bergmann, D. J., Szopa, S., Jonson, J. E., Keating, T. J., and Zuber, A.: Modelling future changes in surface ozone: a parameterized approach, Atmos. Chem. Phys., 12, 2037–2054, doi:10.5194/acp-12-2037-2012, 2012.

Wilkinson, S., Mills, G., Illidge, R., and Davies, W. J.: How is ozone pollution reducing our food supply? J. Exp. Bot., 63, 527–536, doi:10.1093/jxb/err317, 2011.

Wu, S., Mickley, L. J., Jacob, D. J., Rind, D., and Streets, D. G.: Effects of 2000–2050 changes in climate and emissions on global tropospheric ozone and the policy-relevant background surface ozone in the United States, J. Geophys. Res., 113, D18312, doi:10.1029/2007JD009639, 2008a.

Wu, S., Mickley, L. J., Leibensperger, E. M., Jacob, D. J., Rind, D., and Streets, D. G.: Effects of 2000–2050 global change on ozone air quality in the United States, J. Geophys. Res., 113, D06302, doi:10.1029/2007JD008917, 2008b.

Xu, W., Lin, W., Xu, X., Tang, J., Huang, J., Wu, H., and Zhang, X.: Long-term trends of surface ozone and its influencing factors at the Mt Waliguan GAW station, China – Part 1: Overall trends and characteristics, Atmos. Chem. Phys., 16, 6191–6205, doi:10.5194/acp-16-6191-2016, 2016.

Xu, X., Lin, W., Wang, T., Yan, P., Tang, J., Meng, Z., and Wang, Y.: Long-term trend of surface ozone at a regional background station in eastern China 1991–2006: enhanced variability, Atmos. Chem. Phys., 8, 2595–2607, doi:10.5194/acp-8-2595-2008, 2008.

Yang, Y., Liao, H., and Li, J.: Impacts of the East Asian summer monsoon on interannual variations of summertime surface-layer ozone concentrations over China, Atmos. Chem. Phys., 14, 6867–6880, doi:10.5194/acp-14-6867-2014, 2014.

Yang, Y., Liao, H., and Lou, S.: Decadal trend and interannual variation of outflow of aerosols from East Asia: Roles

of variations in meteorological parameters and emissions, Atmos. Environ., 100, 141–153, doi:10.1016/j.atmosenv.2014.11.004, 2015.

Yienger, J. J., and Levy, H.: Empirical model of global soil-biogenic NO_x emissions, J. Geophys. Res., 100, D6, 11447–11464, doi:10.1029/95JD00370, 1995.

Young, P. J., et al.: Preindustrial to end 21st century projections of tropospheric ozone from the Atmospheric Chemistry and Climate Model Intercomparison Project (ACCMIP), Atmos. Chem. Phys., 13, 2063–2090, doi:10.5194/acp-13-2063-2013, 2013.

Yue, X. and Unger, N.: Ozone vegetation damage effects on gross primary productivity in the United States, Atmos. Chem. Phys., 14, 9137–9153, doi:10.5194/acp-14-9137-2014, 2014.

Zhang, L., Jacob, D. J., Boersma, K. F., Jaffe, D. A., Olson, J. R., Bowman, K. W., Worden, J. R., Thompson, A. M., Avery, M. A., Cohen, R. C., Dibb, J. E., Flock, F. M., Fuelberg, H. E., Huey, L. G., McMillan, W. W., Singh, H. B., and Weinheimer, A. J.: Transpacific transport of ozone pollution and the effect of recent Asian emission increases on air quality in North America: an integrated analysis using satellite, aircraft, ozonesonde, and surface observations, Atmos. Chem. Phys., 8, 6117–6136, doi:10.5194/acp-8-6117-2008, 2008.

Zhang, Q., Streets, D. G., Carmichael, G. R., He, K. B., Huo, H., Kannari, A., Klimont, Z., Park, I. S., Reddy, S., Fu, J. S., Chen, D., Duan, L., Lei, Y., Wang, L. T., and Yao, Z. L.: Asian emissions in 2006 for the NASA INTEX-B mission, Atmos. Chem. Phys., 9, 5131–5153, doi:10.5194/acp-9-5131-2009, 2009.

Zhang, Q., Yuan, B., Shao, M., Wang, X., Lu, S., Lu, K., Wang, M., Chen, L., Chang, C.-C., and Liu, S. C.: Variations of ground-level O_3 and its precursors in Beijing in summertime between 2005 and 2011, Atmos. Chem. Phys., 14, 6089–6101, doi:10.5194/acp-14-6089-2014, 2014.

Zhang, Y. C., and Guo, L. L.: Multi-model ensemble simulated changes in the subtropical westerly jet over east Asia under the global warming condition, Scientia Meteorologica Sinica, 30, 694–700, 2010.

Zhou, D., Ding, A., Mao, H., Fu, C., Wang, T., Chan, L. Y., Ding, K., Zhang, Y., Liu J., Lu, A., and Hao, N.: Impacts of the East Asian monsoon on lower tropospheric ozone over coastal South China, Environ. Res. Lett., 8, 044011, doi:10.1088/1748-9326/8/4/044011, 2013.

Zhu, J., and Liao, H.: Future ozone air quality and radiative forcing over China owing to future changes in emissions under the Representative Concentration Pathways (RCPs), J. Geophys. Res. Atmos., 121, 1978–2001, doi:10.1002/2015JD023926, 2016.

Zhu, J. L., Liao, H., and Li, J. P.: Increases in aerosol concentrations over eastern China due to the decadal-scale weakening of the East Asian summer monsoon, Geophys. Res. Lett., 39, L09809, doi:10.1029/2012gl051428, 2012.

Table 1. Anthropogenic emissions[a] of O_3 precursors for the present day (year 2000) and future (year 2050, under the SRES A1B scenario).

Species	Global			Asian[b]		
	2000	2050	Change (%)	2000	2050	Change (%)
NO_x (Tg N yr^{-1})	33.4	59.6	+78.4	10.9	28.3	+159.6
CO (Tg CO yr^{-1})	1054.2	1332.0	+26.4	393.7	487.2	+23.7
NMVOCs (Tg C yr^{-1})	70.8	134.1	+89.4	28.5	62.3	+118.6
CH_4 (ppbv)	1750	2400	+37.1	1750	2400	+37.1

[a] Biomass burning emissions are included.

[b] Asia covers the domain of 60–150 °E, 10 °S–55 °N.

Table 2. Natural emissions of O_3 precursors for the present day (year 2000) and future (year 2050, under the SRES A1B scenario).

Species	Global			Asian[a]		
	2000	2050	Change (%)	2000	2050	Change (%)
Lightning NO_x ($Tg\ N\ yr^{-1}$)	4.8	5.7	+18.8	1.2	1.4	+16.7
Soil NO_x ($Tg\ N\ yr^{-1}$)	6.7	7.7	+14.9	1.4	1.7	+21.4
Biogenic VOCs ($Tg\ C\ yr^{-1}$)	614.5	750.2	+22.1	106.1	126.2	+18.9

[a] Asia covers the domain of 60–150 °E, 10 °S–55 °N.

Table 3. Experimental design of the simulations for 1986–2006.

Simulation	Simulated years	Meteorological parameters	Anthropogenic emissions	CH_4 abundance	Biomass burning emissions
Met	1986–2006	Vary over 1986–2006	Fixed at 2006	Fixed at 2006	Turn off
Emis	1986–2006	Fixed at 2006	Vary over 1986–2006	Vary over 1986–2006	Turn off
MetEmis	1986–2006	Vary over 1986–2006	Vary over 1986–2006	Vary over 1986–2006	Turn off
MetEmisB[a]	1997–2006	Vary over 1997–2006	Vary over 1997–2006	Vary over 1997–2006	Vary over 1997–2006

[a] The MetEmisB simulation is conducted for 1997–2006 owing to the unavailability of biomass burning emissions before 1997.

Table 4. Information for the sites with O_3 measurements used in model evaluation.

Site	Location	Database	Height	R[a]	NMB[b] (%)
Minamitorishima	24.3 °N, 154.0 °E	WDCGG	surface	0.92	+12.7
Yonagunijima	24.5 °N, 123.0 °E	WDCGG	surface	0.93	+12.6
Rishiri	45.1 °N, 141.2 °E	EANET	surface	0.82	+2.4
Ogasawara	27.1 °N, 142.2 °E	EANET	surface	0.90	+29.6
Naha	26.2 °N, 127.7 °E	WOUDC	500–300 hPa	0.68	–2.61
			700–500 hPa	0.77	+16.4
			850–700 hPa	0.85	+24.3
			1000–850 hPa	0.88	+39.5
Tsukuba	36.1 °N, 140.1 °E	WOUDC	500–300 hPa	0.55	+15.8
			700–500 hPa	0.76	+12.3
			850–700 hPa	0.76	+8.61
			1000–850 hPa	0.60	+8.5

[a] Correlation coefficient (R) between the observed and simulated monthly O_3 mixing ratios.

[b] Normalized mean bias (NMB, %) between the observed and simulated monthly O_3 mixing ratios.

Table 5. Simulated present-day O_3 fluxes and projected changes from the present day (1996–2005) to the future (2046–2055) through the vertical plane along 135 °E from 20 °N to 55 °N, and from the surface to 100 hPa, due to future climate change alone, change in anthropogenic emissions alone, and changes in both climate and emissions.

	O_3 Fluxes[a]			
	Met2000Emis2000 (present day)	Met2050Emis2000 (climate)	Met2000Emis2050 (emissions)	Met2050Emis2050 (climate + emissions)
DJF	792.9	778.3 (−1.8%)	850.5 (+7.3%)	853.7 (+7.7%)
MAM	597.0	640.4 (+7.3%)	639.0 (+7.0%)	698.0 (+16.9%)
JJA	146.5	167.7 (+14.5%)	161.3 (+10.1%)	187.2 (+27.8%)
SON	340.7	327.8 (−3.8%)	374.1 (+9.8%)	368.1 (+8.0%)
Annual	1877.1	1914.1 (+2.0%)	2024.9 (+7.9%)	2106.9 (+12.2%)

[a] The units are Tg season^{-1} for seasonal fluxes and Tg yr^{-1} for annual fluxes. Values in parentheses are percentage changes relative to the present-day fluxes.

Figure captions

Figure 1. Evolution of annual anthropogenic and biomass burning emissions summed over the globe and Asia (60–150 ° E, 10 ° S–55 ° N) for NO_x (Tg N yr^{-1}), CO (Tg CO yr^{-1}), and NMVOCs (Tg C yr^{-1}) over 1986–2006. Blue squares represent anthropogenic emissions, and red circles represent the sum of anthropogenic emissions and biomass burning emissions. The last panel shows the evolution of global CH_4 abundance (ppbv) during 1986–2006.

Figure 2. Evolution of annual natural emissions summed over the globe and Asia (60–150 ° E, 10 ° S–55 ° N) for lightning NO_x (Tg N yr^{-1}), soil NO_x (Tg N yr^{-1}), and biogenic VOCs (Tg C yr^{-1}) over 1986–2006.

Figure 3. Time series of monthly surface-layer O_3 mixing ratios measured by WDCGG and EANET (blue line), and simulated by MetEmisB (red line). (a) Minamitorishima and (b) Yonagunijima are WDCGG sites, and (c) Rishiri and (d) Ogasawara sites are EANET sites.

Figure 4. Time series of monthly O_3 mixing ratios measured by ozonesonde (blue line), and simulated by MetEmisB (red line). (a) Naha and (b) Tsukuba are ozonesonde sites from WOUDC. Comparisons are shown for four altitude levels in the troposphere.

Figure 5. Comparison of simulated trends in seasonal or annual mean surface-layer O_3 concentrations from the MetEmis experiment with observations for Hongkong (location: 22.2 °N, 114.3 °E; years: 1994–2007; reference: Wang et al., 2009b), Waliguan (36.3 °N, 100.9 °E; 1994–2013; Xu et al. 2016), Beijing (40.0 °N, 116.5 °E; 2001–2006; Tang et al., 2009), and Taiwan (23.5 °N, 121.0 °E; 1994–2007; Lin et al., 2010). The simulated trend at Waliguan site for winter is statistically insignificant. The trends in seasonal-mean O_3 concentrations at Taiwan station are unavailable.

Figure 6. The pressure–latitude cross-sections along 135 ° E of the simulated seasonal O_3 outflow fluxes and zonal winds during four seasons averaged over 1997–2006 in the MetEmisB simulation. The O_3 mass fluxes are shown by shades (units: kg $season^{-1}$ m^{-2}), and winds are represented by contours (units: m s^{-1}). Positive fluxes represent eastward fluxes, and negative values represent westward fluxes.

Figure 7. Evolution of (a) annual O_3 outflow fluxes (Tg yr^{-1}) across the meridional plane along 135 °E from 20 °N to 55 ° N, and from the surface to 100 hPa, over 1986–2006 in the Met, Emis, and MetEmis simulations; (b) the associated deviations from the mean (%); and (c) deviations from the mean (%) of the detrended O_3 outflow fluxes. The deviation from the mean (DEV) is defined in Sect. 4.2.

Figure 8. The MAD and APDM values of the detrended seasonal and annual O_3 outflow fluxes across the meridional plane along 135 °E from 20 °N to 55 °N, and from the surface to 100 hPa, over 1986–2006 in Met, Emis, and MetEmis simulations. Both the MAD and APDM are defined in Sect. 4.2. The units of MAD are Tg $season^{-1}$ for seasonal fluxes and Tg yr^{-1} for annual fluxes.

Figure 9. The pressure–latitude cross-sections along 135 ° E of MAD values for detrended annual O_3 outflow fluxes and zonal winds over 1986–2006 in the Met, Emis, and MetEmis simulations. The MAD values for O_3 mass fluxes are shown by shades (units: kg yr^{-1} m^{-2}), and the MAD values for winds are represented by contours (units: m s^{-1}).

Figure 10. (a) The pressure–latitude cross-sections along 135 ° E of simulated present-day O_3 mass fluxes and zonal winds (Met2000Emis2000). Projected changes in O_3 mass fluxes and zonal winds from the present day (1996–2005) to the future (2046–2055) caused by (b) climate change alone (Met2050Emis2000 minus Met2000Emis2000); (c) changes in anthropogenic emissions alone (Met2000Emis2050 minus Met2000Emis2000); and (d) changes in both

climate and anthropogenic emissions (Met2050Emis2050 minus Met2000Emis2000). The O_3 mass fluxes are shown by shades (units: kg season^{-1} m^{-2}), and winds are represented by contours (units: m s^{-1}). The dotted areas are statistically significant at the 95 % level, as determined by a two-sample Student's *t*-test.

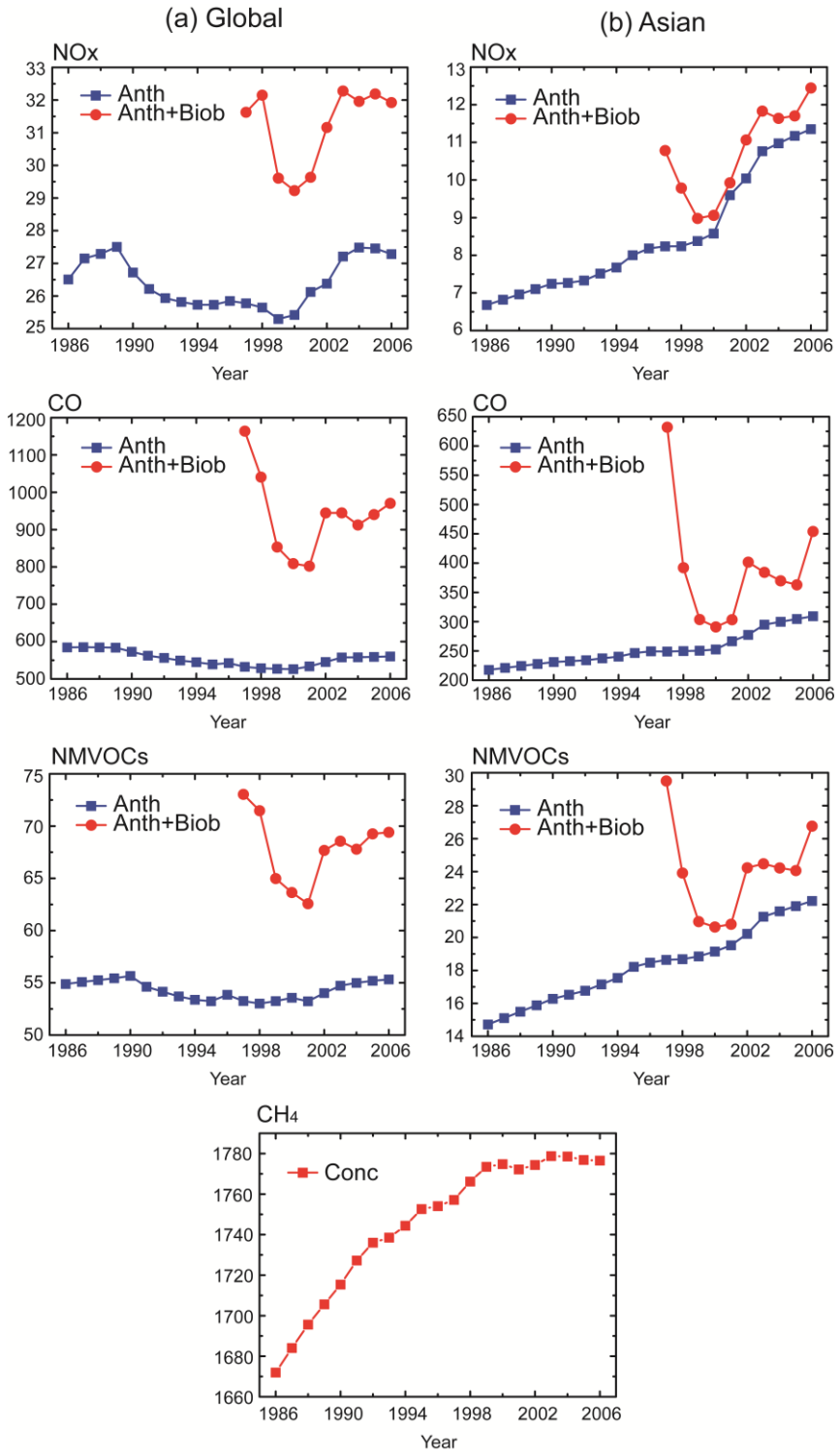

Figure 1. Evolution of annual anthropogenic and biomass burning emissions summed over the globe and Asia (60–150 ° E, 10 ° S–55 ° N) for NO_x (Tg N yr^{-1}), CO (Tg CO yr^{-1}), and NMVOCs (Tg C yr^{-1}) over 1986–2006. Blue squares represent anthropogenic emissions, and red circles represent the sum of anthropogenic emissions and biomass burning emissions. The last panel shows the evolution of global CH_4 abundance (ppbv) during 1986–2006.

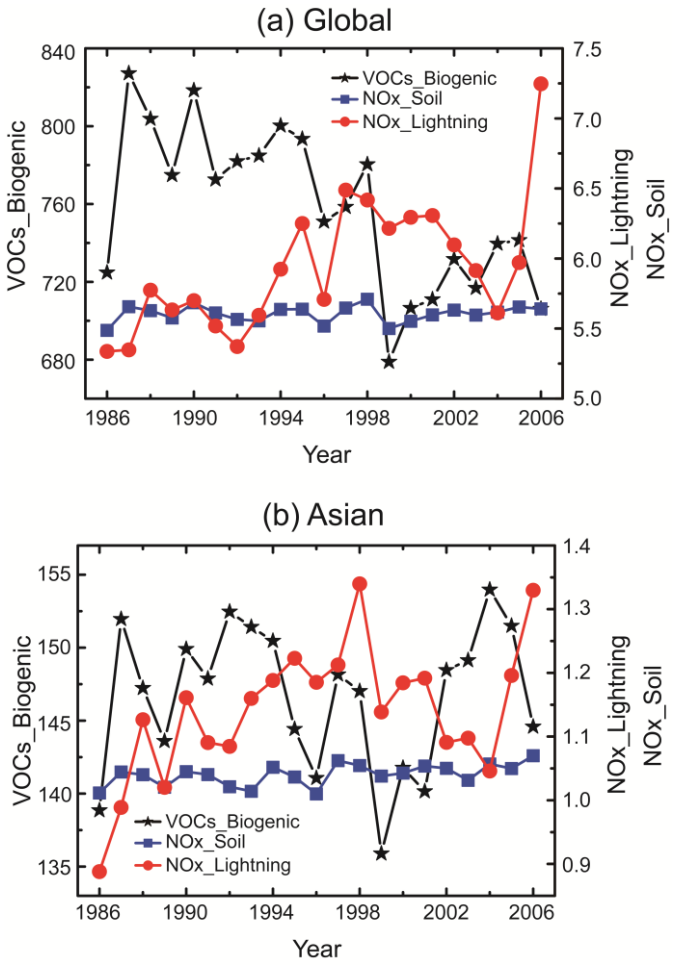

Figure 2. Evolution of annual natural emissions summed over the globe and Asia (60–150 ° E, 10 ° S–55 ° N) for lightning NO_x (Tg N yr^{-1}), soil NO_x (Tg N yr^{-1}), and biogenic VOCs (Tg C yr^{-1}) over 1986–2006.

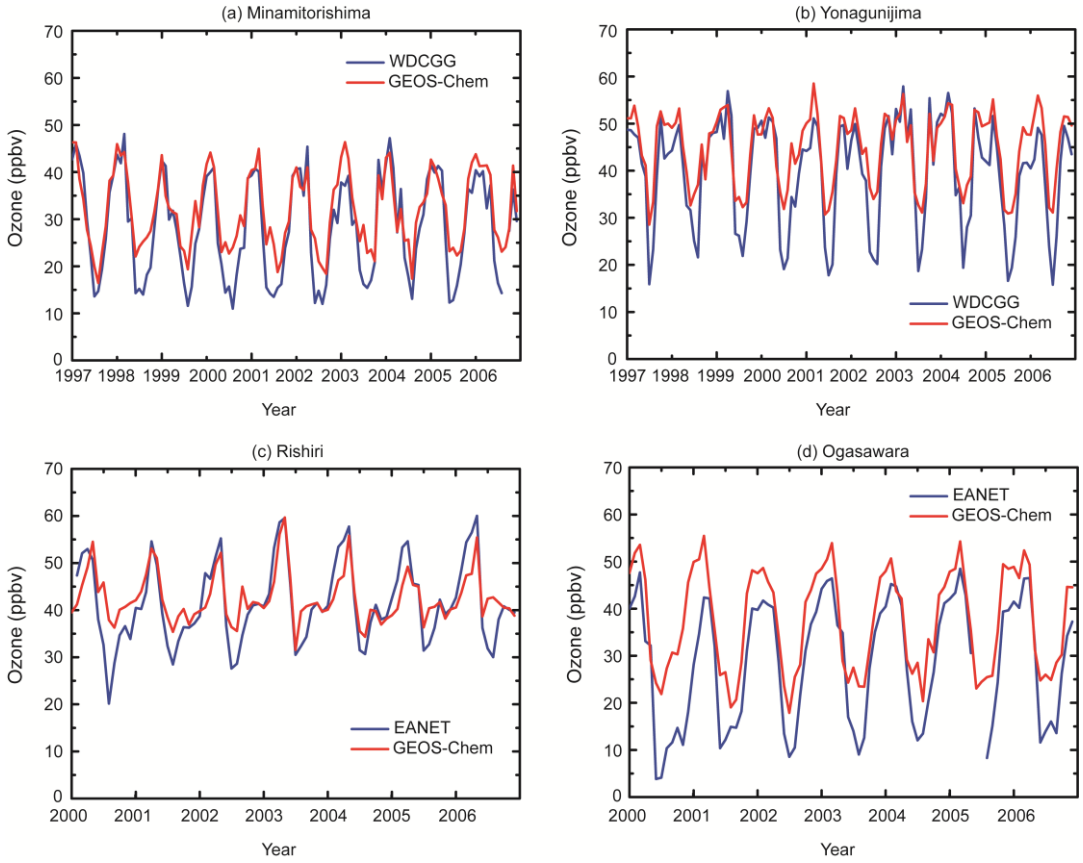

Figure 3. Time series of monthly surface-layer O_3 mixing ratios measured by WDCGG and EANET (blue line), and simulated by MetEmisB (red line). (a) Minamitorishima and (b) Yonagunijima are WDCGG sites, and (c) Rishiri and (d) Ogasawara sites are EANET sites.

5

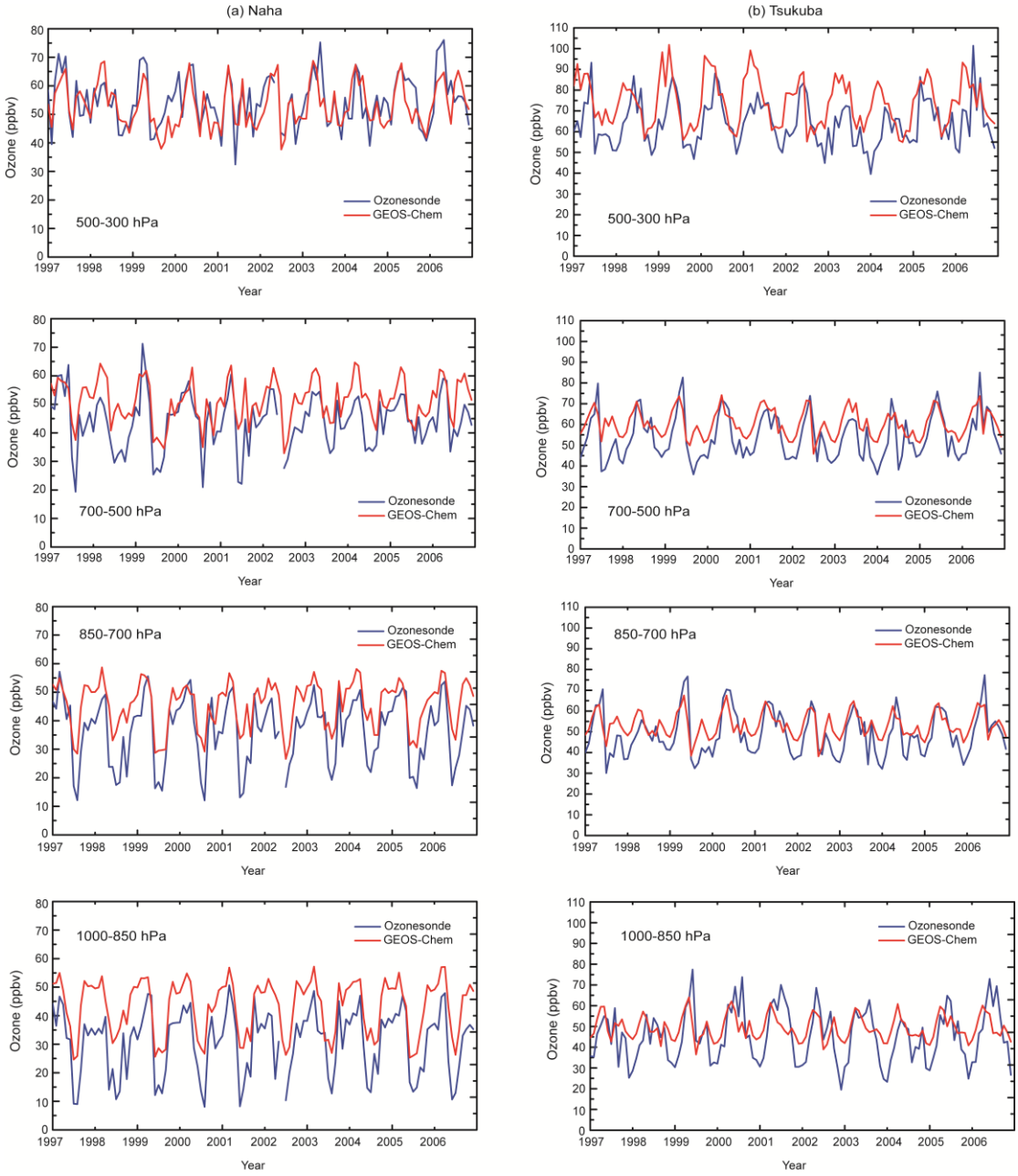

Figure 4. Time series of monthly O_3 mixing ratios measured by ozonesonde (blue line), and simulated by MetEmisB (red line). (a) Naha and (b) Tsukuba are ozonesonde sites from WOUDC. Comparisons are shown for four altitude levels in the troposphere.

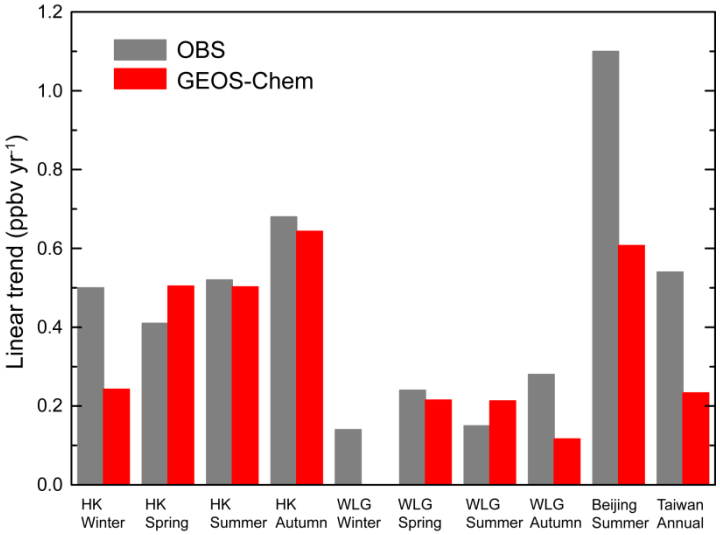

Figure 5. Comparison of simulated trends in seasonal or annual mean surface-layer O_3 concentrations from the MetEmis experiment with observations for Hongkong (location: 22.2 ° N, 114.3 ° E; years: 1994–2007; reference: Wang et al., 2009b), Waliguan (36.3 °N, 100.9 °E; 1994–2013; Xu et al. 2016), Beijing (40.0 °N, 116.5 °E; 2001–2006; Tang et al., 2009), and Taiwan (23.5 °N, 121.0 °E; 1994–2007; Lin et al., 2010). The simulated trend at Waliguan site for winter is statistically insignificant. The trends in seasonal-mean O_3 concentrations at Taiwan station are unavailable.

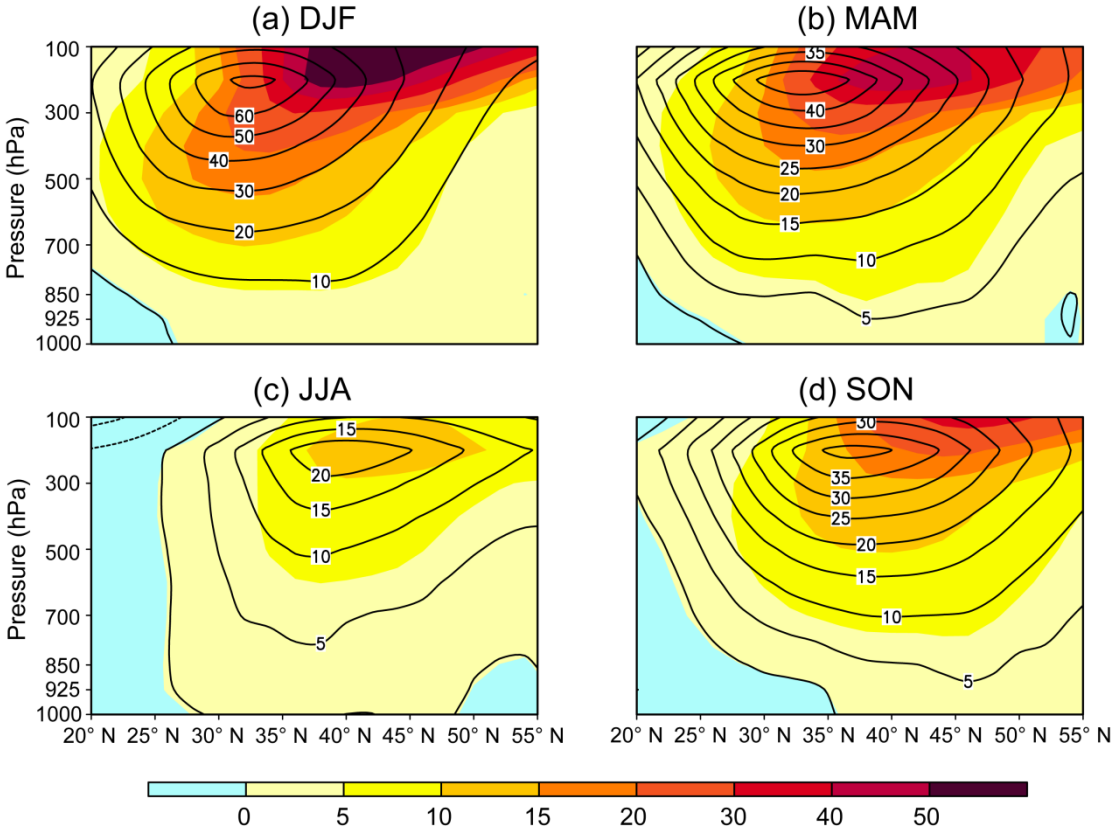

Figure 6. The pressure–latitude cross-sections along 135 ° E of the simulated seasonal O_3 outflow fluxes and zonal winds during four seasons averaged over 1997–2006 in the MetEmisB simulation. The O_3 mass fluxes are shown by shades (units: kg season^{-1} m^{-2}), and winds are represented by contours (units: m s^{-1}). Positive fluxes represent eastward fluxes, and negative values represent westward fluxes.

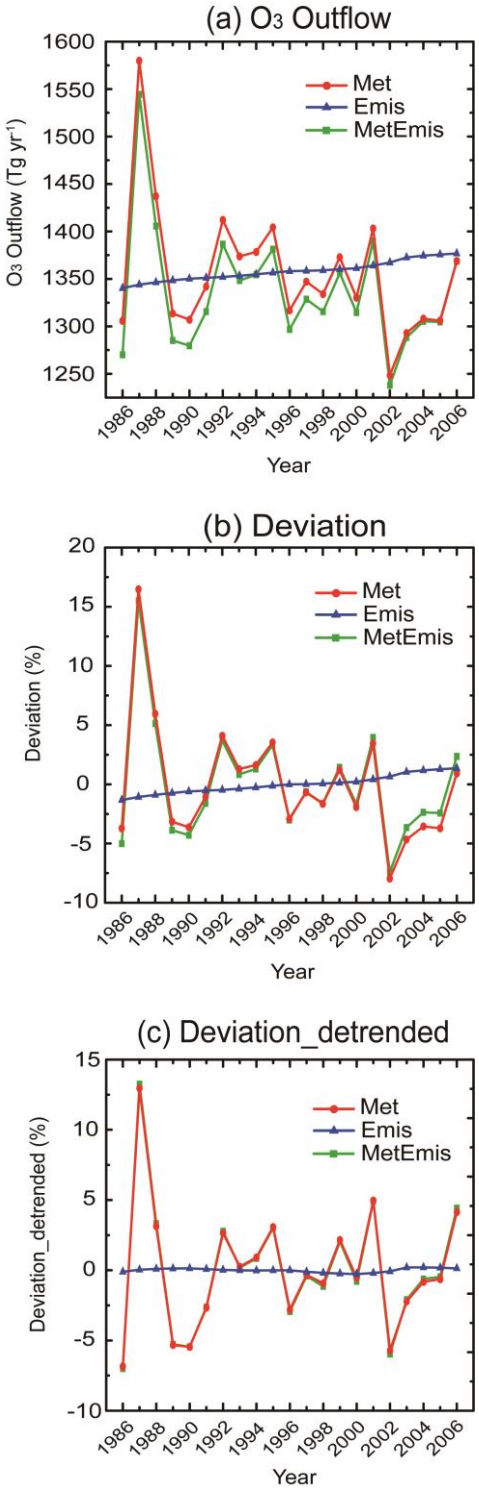

Figure 7. Evolution of (a) annual O_3 outflow fluxes (Tg yr^{-1}) across the meridional plane along 135 °E from 20 °N to 55 ° N, and from the surface to 100 hPa, over 1986–2006 in the Met, Emis, and MetEmis simulations; (b) the associated deviations from the mean (%); and (c) deviations from the mean (%) of the detrended O_3 outflow fluxes. The deviation from the mean (DEV) is defined in Sect. 4.2.

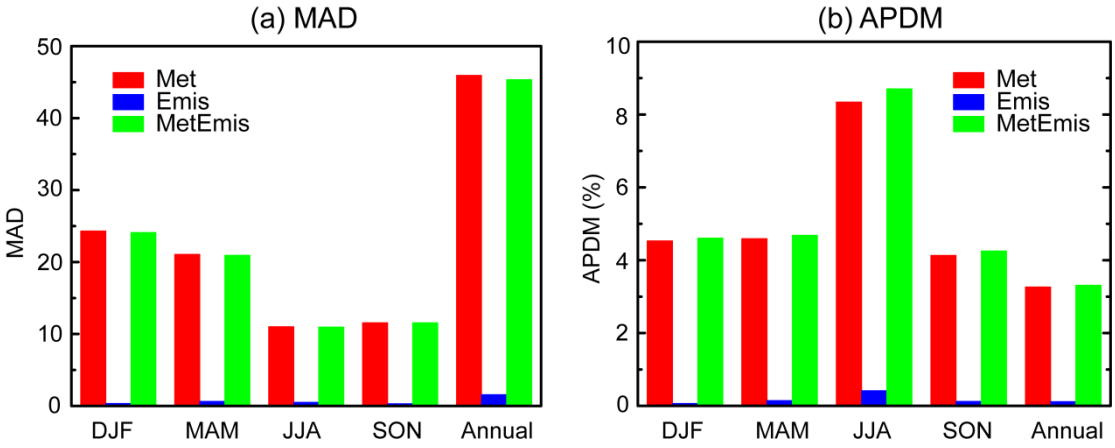

Figure 8. The MAD and APDM values of the detrended seasonal and annual O_3 outflow fluxes across the meridional plane along 135 °E from 20 °N to 55 °N, and from the surface to 100 hPa, over 1986–2006 in Met, Emis, and MetEmis simulations. Both the MAD and APDM are defined in Sect. 4.2. The units of MAD are Tg season^{-1} for seasonal fluxes and Tg yr^{-1} for annual fluxes.

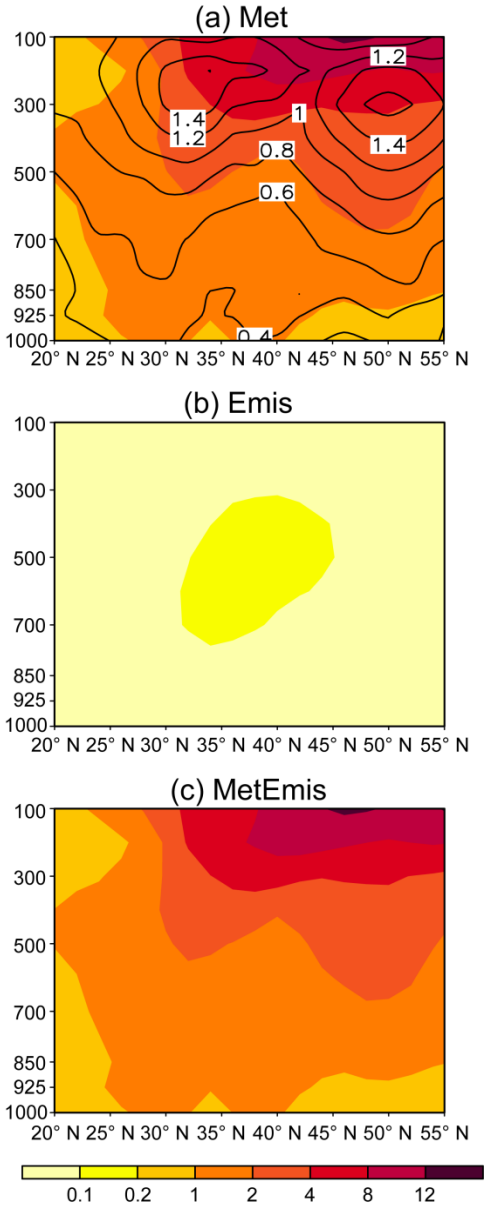

Figure 9. The pressure–latitude cross-sections along 135 °E of MAD values for detrended annual O_3 outflow fluxes and zonal winds over 1986–2006 in the Met, Emis, and MetEmis simulations. The MAD values for O_3 mass fluxes are shown by shades (units: kg yr^{-1} m^{-2}), and the MAD values for winds are represented by contours (units: m s^{-1}).

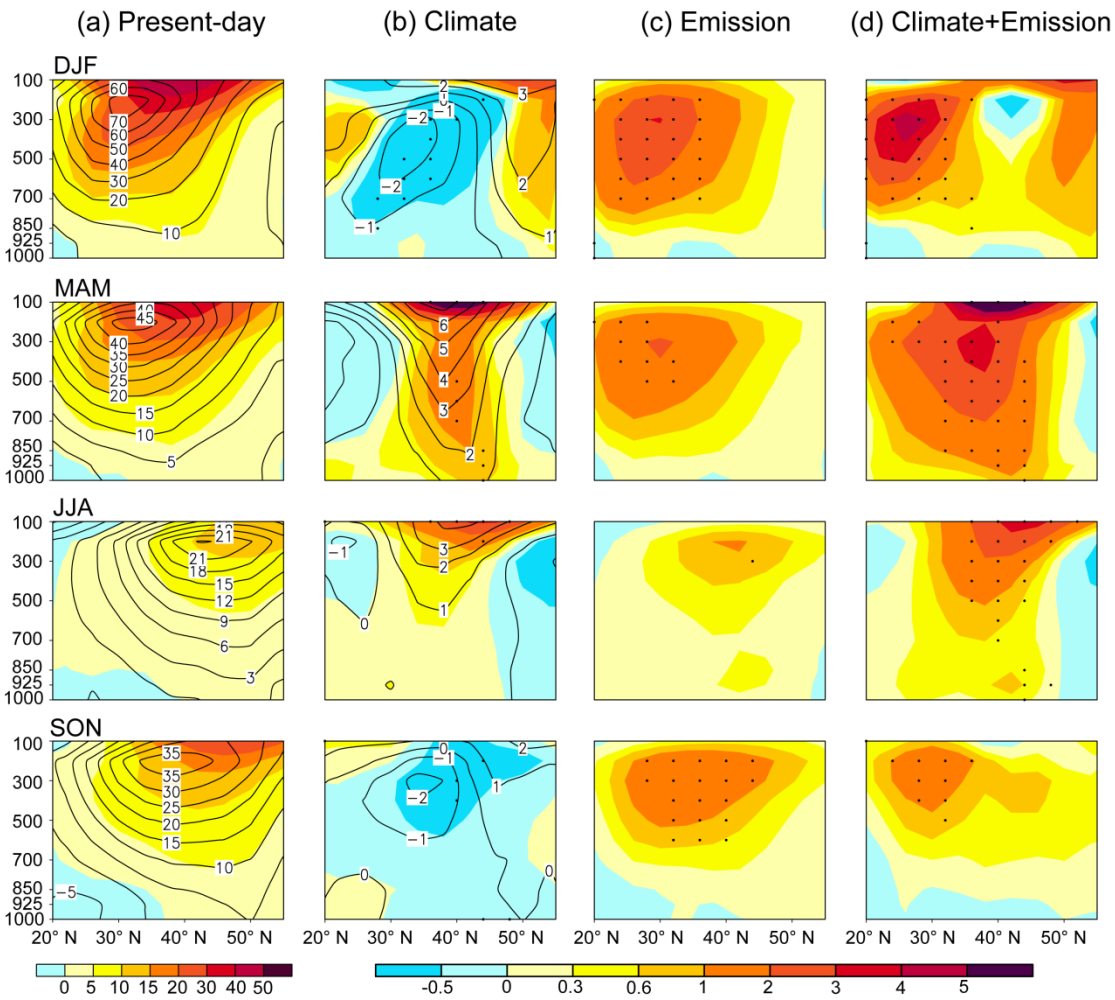

Figure 10. (a) The pressure–latitude cross-sections along 135 °E of simulated present-day O_3 mass fluxes and zonal winds (Met2000Emis2000). Projected changes in O_3 mass fluxes and zonal winds from the present day (1996–2005) to the future (2046–2055) caused by (b) climate change alone (Met2050Emis2000 minus Met2000Emis2000); (c) changes in anthropogenic emissions alone (Met2000Emis2050 minus Met2000Emis2000); and (d) changes in both climate and anthropogenic emissions (Met2050Emis2050 minus Met2000Emis2000). The O_3 mass fluxes are shown by shades (units: kg season^{-1} m^{-2}), and winds are represented by contours (units: m s^{-1}). The dotted areas are statistically significant at the 95 % level, as determined by a two-sample Student's *t*-test.